Effects of Sputtered Platinum Counter Electrode and Integrated TiO_2 Electrode with SWCNT on DSSC Performance

by

Kartik Kinhal

A Thesis Presented in Partial Fulfillment
of the Requirements for the Degree
Master of Science in Technology

Approved November 2011 by the
Graduate Supervisory Committee:

Lakshmi Munukutla, Chair
Xihong Peng
James Subach

ARIZONA STATE UNIVERSITY

December 2011

ABSTRACT

Dye sensitized solar cells (DSSCs) are the third generation solar cells expected to outperform the first two generations of solar cells with their advantages of comparative higher efficiency and lower manufacturing costs. The manufacturing cost of Dye sensitized solar cells is one fifth of the conventional silicon solar cell. However, DSSCs have problems of low conversion efficiency, stability and reliability. Some effective approaches are required to improve their performance. This paper projects the work related to assessment and verification of the repeatability of the semi-automated fabrication process. Changes were introduced in to the fabrication process to enhance the efficiency and stability. The sealant step in the fabrication process was remodeled to a newer version with an improvement in efficiency from 11% to 11.8%. Sputtering was performed on counter electrode in 30 seconds intervals. Cells were fabricated to assess the performance & time dependent characteristics from EIS experiments. Series resistance increased three times in sputtered Pt electrode as compared to standard platinum electrode. This resulted in the degradation of conductive surface on glass electrode due to heavy bombardment of ions. The second phase of the project work relates to the incorporation of SWCNT on the TiO_2 electrode and its effect on the cell efficiency. Different weight loadings (0.1 wt %, 0.2 wt%, 0.4 wt %) of SWCNTs were prepared and mixed with the commercial TiO_2 paste and ethanol solvent. The TiO_2-SWCNT layer was coated on the electrode using screen-printing technique. Both open circuit voltage and photocurrent were found to have measurable dependence on the TiO_2 layer loading. Photo voltage ranged from ~0.73 V to ~0.43 V and photocurrent from ~8 to ~33 mA depending on weight percent loading. This behavior is due to aggregation of particles and most TiO_2 aggregate particles are not connected to SWCNT. Transparency loss was observed leading to saturation in the photo current and limiting the light absorption within the TiO_2 film.

Dedicated To

My both grandmothers

And

Parents for their everlasting love & support.

ACKNOWLEDGMENTS

First and the foremost, I would like to express my sincere gratitude to my graduate committee chair, Dr. Lakshmi Munukutla, who has been instrumental in guiding me towards the successful completion of my project. I sincerely thank her for her invaluable guidance, support and encouragement in undertaking this quality research. I am immensely grateful to the committee members, Dr. James Subach and Dr. Xihong Peng, for their support and guidance, not only for the thesis work, but also for their invaluable advice throughout my graduate coursework.

I earnestly thank Dr. Arunachalanadar Madakannan for his extensive support and invaluable guidance ensuring that I am always on the right track in my thesis work and also by providing the resources & facilities in the Alternative energy lab.

I would like to thank Arizona State University for providing me an opportunity to pursue the Masters' degree, and all the faculty and staff of the Engineering Technology Department for all their assistance during my stay at ASU.

My special thanks are due to Stefan Myhajlenko for his continuous assistance while performing the characterization studies with the scanning electron microscope.

I would like to express my gratitude to Mr. Scott Adams from chemistry department at ASU for providing necessary machine & equipment in a short interval of time which was required for the completion of the project.

I would like to thank my fellow graduate students Rashida Villacorta, QuratulAin Shah, Shawn Liu, Anthony Adame and Aditi Jhalani for their help in accomplishing this research.

I am also grateful to Yen-shih-Huang, Chih Yu Jen, Aung Htun, Sailaja Radhakrishnan, Brian Fauss and Laura Main, Rene Fischer, Carl Villanueva & Martha Benton for their multifarious support and encouragement. Last but not the least I thank all my friends and relatives for their continuous encouragement.

TABLE OF CONTENTS

Page

CHAPTER Page

LIST OF TABLES

LIST OF FIGURES

Figure Page

Figure Page

1. INTRODUCTION

1.1 Advances in Technology

The emergence of an electric potential between two electrodes attached to a solid or liquid system upon light irradiation has been discovered by Becquerel in 1839 [1] and is known as photovoltaic effect. This discovery became the foundation for a variety of concepts to convert solar radiation into electricity, and a new domain of alternative energy generation.

The photovoltaic market is dominated by silicon in its multicrystalline and mono crystalline forms. Silicon research is concentrated on thin-film crystalline silicon (about 5–30 μm active layer thickness), that avoids the costly crystal growing and sawing processes. The problems associated with this material are: assuring adequate light absorption, good crystal quality and purity of the films, and finding a substrate that fulfills all these requirements. Genuine thin-film materials with thickness of up to 1 μm are characterized by direct band structure, which facilitates higher light absorption. Other inorganic materials used for the photovoltaic devices belong to the group of chalcogenides such as copper indium diselenide (CIS) and cadmium telluride. Exploration has even expanded to CuInSe2 to CuGaSe2, CuInS2 and their multinary alloys Cu (In, Ga) $(S, Se)_2$.

Laboratory efficiencies for smaller area devices are approaching 19 % and large area modules have reached 12 %. Cadmium telluride solar cells showing slightly lower efficiency, offer great promise. From a solid-state physics point of view, silicon is not an ideal material for photovoltaic conversion for two reasons: small spectral mismatch between absorption, semiconductor and the sunlight spectrum, approximated by a black body at 5900 K. A much more serious point is that silicon is an indirect gap semiconductor, resulting in valence band maximum and conduction band minimum are not aligned in k-space. Light absorption is much weaker in an indirect gap semiconductor than in a direct band gap semiconductor.

This has serious consequences from materials point of view: for a 90 % light absorption it takes only 1 μm of GaAs (a direct band gap semiconductor) versus 100 μm of Si. The photo-generated carriers have to reach the pn-junction, which is near the front surface. The desirable diffusion length of minority carriers has to be 200 μm or at least twice the silicon thickness. Thus, the material has to be of very high purity accompanied by high crystalline perfection. In view of these physical limitations, a lot of effort has been invested into the search for new materials. Consequently the band gap requirements for the ideal solar cell material are between 1.1 and 1.7 eV for a direct band structure. Furthermore the material should be readily available, non-toxic and processible with easy reproducible deposition techniques suitable for large area production. Alternatively other device geometries have been developed to convert light to electron, such as concentrating systems including III/V-tandem cells.

Additionally, the search for new materials has extended into the field of organic molecules and polymers, which offer several advantages compared to inorganic materials. Organic materials are chemically tunable to adjust physical properties such as band gap, valence, conductivity, charge transport, solubility, and morphological properties. In general, their processing is easier and is established by using wet-processing techniques (spin coating, cast coating, ink-jet printing, roll-to-roll processing) as well as dry processing (thermal evaporation). Due to the small quantities needed for device preparation and the ease of large scale production and purification, organic materials offer an economic advantage over inorganic materials. Organic photovoltaic solar cells bear greater potential for the development of low-cost modules for production of domestic electricity. Organic charge transport materials have either molecular or polymer structure. While charge transport in molecular systems occurs inter molecularly, polymer charge transport proceeds intramolecularly, along the polymer chain. Both technologies show some advantages and comparable device performances.

Molecular and polymer organic materials found application in solar cells of different geometrical structure [2, 3]. In the single layer or Schottky junction cell, the light

absorption semiconductor is forming a rectifying junction with one electrode, which allows the charge separation [4]. Absorption covering the entire visible range is rare using a single species of molecules. Since positive and negative photo excited charges travel through the same material, recombination losses are high for this cell structure. In contrast double layer cells offer separate charge transport layers and therefore, less recombination take place [5]. Light absorption and the generation of electron-hole pairs (excitons) are limited to a small interface layer. Only excitons (electron-hole pairs) of a thin layer, corresponding to the sum of excitons diffusion length and depletion layer thickness, get dissociated. The interface between two materials is drastically increased in the interpenetrated network of layer blend systems. A special type of layer blend device is the dye-sensitized solar cell. Classical dye-sensitized solar cells are hetero-junction devices between an inorganic large band gap semiconductor and an electrolyte. However, the classification of dye-sensitized solar cells into the group of organic solar cells is due to an organic dye molecule adsorbed onto the semiconductor surface, sensitizing the semiconductor for visible light absorption. Several derivatives of this type of device, employing inorganic sensitizers, such as inorganic quantum dots are subject of recent research.

The mobility of carriers is the major limitation in extensive application of photovoltaic devices. Mobility in organic semiconductors is usually small (10-2 cm^2/sV) and in well-ordered conjugated polymers down to 10-8 cm^2/sV in guest polymer systems, and for molecular systems, it's even lower. A mobility distribution for a given material causes a dispersive charge transport. Mobilities are highly dependent on the electric field and the molecular packing quality, which is determined by molecular ordering. Correspondingly, a drastic reduction of mobility will be caused by imperfect purification and uncontrolled crystallization [6] as well as oxygen traps [7]. Another problem, in particular for earlier organic photovoltaic devices, is the degradation of the organic material, which might have several causes. Electrochemical reactions, caused by ionic impurities and/or water, which may promote redox reactions at an electrode, for example,

can be addressed by employing highly purified materials and encapsulation of the device. Degradation due to structural reorganization processes, such as re-crystallization of glasses on heating of the sample were controlled by engineering sterically demanding molecule structures. Photochemical reactions in a charge transport material, however, are more difficult to control. Although organic solar cells cannot compete with conventional photovoltaic cells in commercial application, the prospective to develop a long-term technology based on environmentally safer materials with unlimited availability justifies intensive research in this field.

1.2 The Energy Crunch

With excessive industrialization in developed countries and increase in the standard of living in developing countries, average worldwide power consumption is expected to rise to 30 terawatts by 2050. Climate change and global sustainability have become the convergence points in the global negotiations. Currently fossil fuels dominate the worldwide energy use. Demand for fossil fuels will exceed annual production soon resulting in economic and political crises and conflicts. The use of fossil fuels is confronted with problems of environmental degradation and climate change effects demanding a shift to renewable energy sources. According to World Economic Council Report [8], the share of renewable energy sources is expected to grow by 56% over the next 24 years. A major contribution to this transition is expected to come from solar energy. Political assertions from all across are forcing a quicker transition through better technologies. Series of Climate conventions have put pressure on the scientific community to improve the alternative energy efficiency to curb global emissions. Since solar energy is the most abundant energy resource available, generating the electricity by using solar cells is one of the best ways to reduce the usage of fossil fuels, thereby reducing the CO_2 emission. However, the solar cell technology is currently marred by high production cost. Besides, the efficiency of most widely used crystalline silicon (c-Si) solar cells today is around 13% and its electricity generation cost of $0.30/kW-hr is much higher than electricity generation cost of gas turbine, which is around $0.06/kW-hr.

Figure 1.1, provides a comparison of the best research-cell efficiency between different types of solar cells [9]. Multi-junction solar cell has achieved a record efficiency of 40.7% as compared to 20-27% of crystalline solar cells. However, the cost of fabrication of multi-junction concentration solar cells is three times higher than the cost of gasoline. DSSCs, which possess the simple fabrication procedure and promising applications on flexible substrates, are considered as third generation solar cells [9].

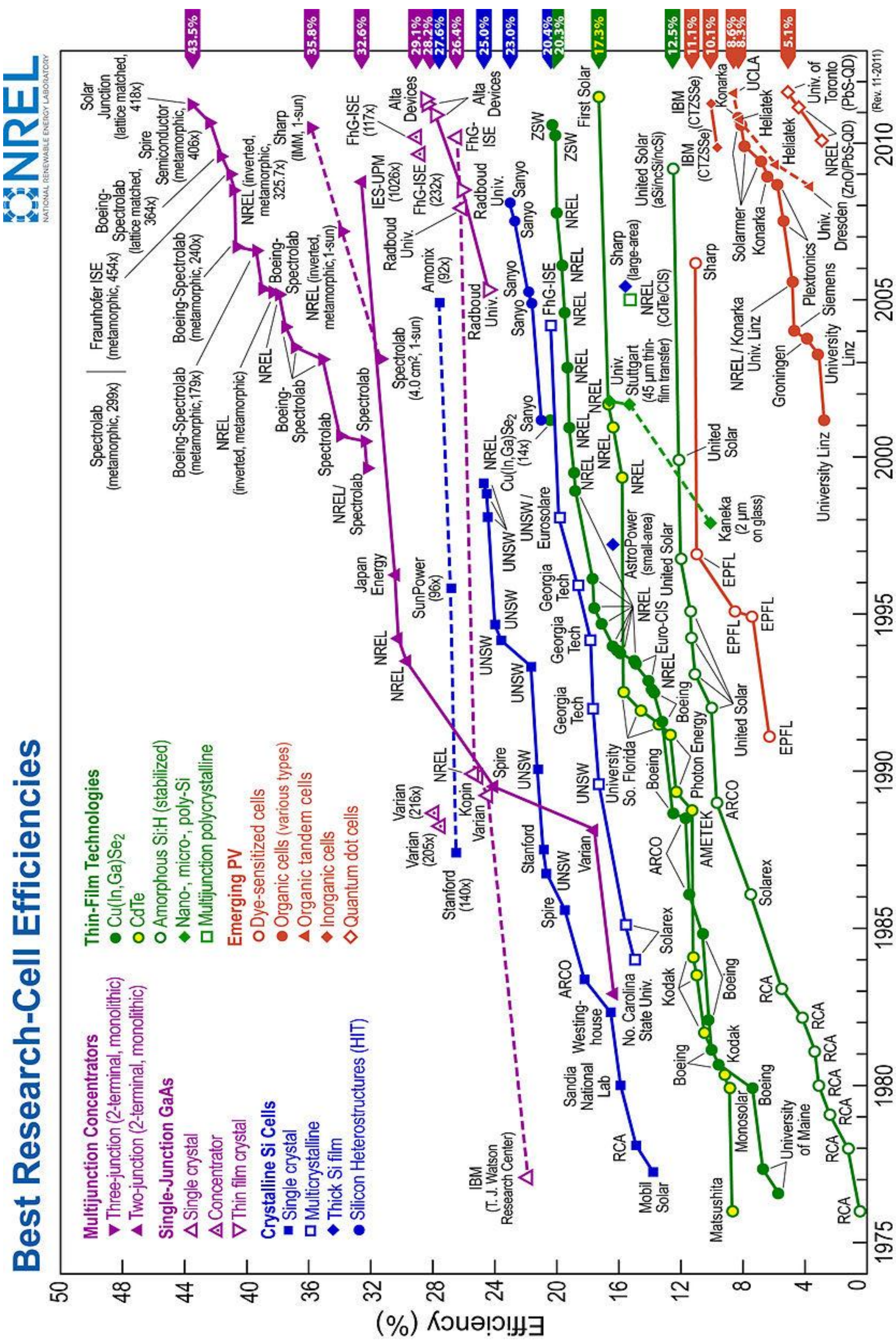

Fig 1.1 – Research cell efficiency trend [9]

The cost of the third generation solar cell (DSSCs) is predicted to be one-fifth that of the conventional solar cell (silicon solar cells). The recorded efficiency of 11.2% for the DSSCs has been reported by Y. Chiba et.al. [10].

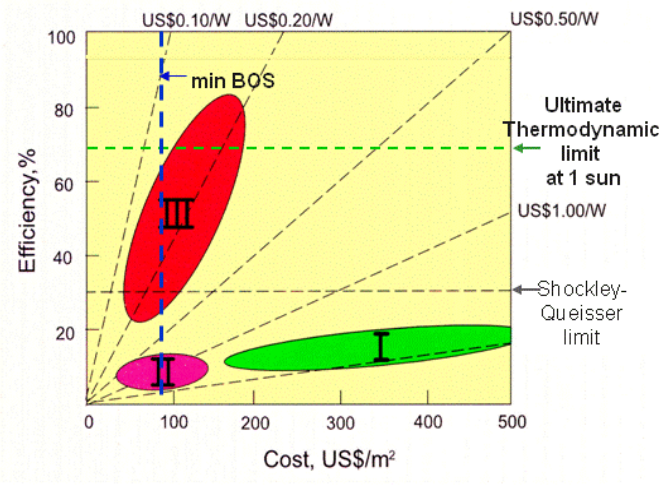

Fig. 1.2: Cost comparison of solar cell generations (Note I – Monocrystalline Cells, II – Polycrystalline cells, III – Thin film cells) [9]

1.3 Solar cells

The variety of solar cell types and applications build scope for finding a solution to energy problem. The solar cells are broadly classified into crystalline silicon cells and thin layer cells. The most preferred solar cell type is conventional silicon solar cell. The crystalline cells are further divided into polycrystalline cells, polycrystalline power cells, polycrystalline band cells and polycrystalline thin line cells. The thin layer cells are classified into amorphous silicon cells, copper-indium diselenide (CIS), Cadmium Telluride cells (CdTe), Dye cell, microcrystalline and micromorphous cells.

In conventional silicon solar cells, two types of crystals are used; n-doped, with a free electron to move and p-doped with no electron. When these two crystals are combined, the free electron tends to move from n-doped crystal to the p-doped crystal to fill the missing electron, named as electron hole. As soon as solar radiation hits the surface of the cell, photons in the light excite the valence electrons of p-doped crystals and this photo excited free electron moves to the n-doped crystal. Repeated transfer of

electron from n-doped crystal to p- doped crystal to fill the electron hole produces current by using the solar radiation.

A typical crystalline silicon cell is composed of two kinds of silicon layers; one where sun light hits, which is negatively doped with Phosphorus and the second is positively doped with Boron. At the boundary layer of two layers, charge separation occurs. Besides, a metallic contact is used on the front and back sides of the cell to take the power to outside of the cell. For instance, some of the freshly ejected electrons from p-doped area are taken from the other p-doped crystals in the system. Besides, because some photons have a higher energy than the required energy for photo excitement, remained energy transformed to heat after the photo excitement. Also, silicon is an expensive material and many practical obstacles exist to reduce the cost of processing silicone [11]. Most common semiconductor material is silicon but gallium, cadmium, tellurium and copper can be used in photovoltaic cells. Many types of PV exist but crystalline solar cells are the most preferred ones.

Since the 1990s, there has been an increase in development of thin-film processes for manufacturing solar cells. In these, photoactive semiconductors are applied as thin layers to a low-cost substrate (in most cases, glass). The methods used include vapor deposition; sputter processes (cathode sputtering) and electrolytic baths. Amorphous silicon, copper indium diselenide (CIS) and cadmium telluride (CdTe) are used as semiconductor materials. Because of the high light absorption of these materials, layer thicknesses of less than 0.001 mm are theoretically sufficient for converting sunlight to electrical energy. The materials are more tolerant to contamination by foreign atoms. Compared to manufacturing temperatures of up to 1500°C for crystalline silicon cells, thin-film cells require deposition temperatures of between 200°C and 600°C. The capability of thin film technology for highly automated production with a large throughput offers considerable saving potentials when compared to crystalline silicon technology. Thin-film cells are not restricted in their format to standard wafer sizes, as is the case with crystalline cells. Theoretically, the substrate can be cut to any size and coated with

semiconductor material. However, because only cells of the same size can be connected in series for internal wiring, practically only rectangular formats are commonly used. A further distinguishing feature of thin-film cells that differentiates them from crystalline cells is the way in which they are connected together. While crystalline solar cells are soldered together from cell to cell (external interconnection), thin-film cells are interconnected monolithically during the coating and layering process. The cells are electrically separated and interconnected by means of structuring stages, in which each cell layer is cut into strip-like individual cells. [42]

This creates thin transparent grooves between individual cells. In order to achieve high energy yield, they are made as thin as possible and are not visible to the naked eye. They can, however, be used as a design element and be deliberately widened. The wider the grooves between the cells, the greater the transparency. The semi-transparent optical effect can also be created by forming additional grooves perpendicular to the cell strips. The electrical contact is created on the back with an opaque metal coating. On the front side facing the light, this function is fulfilled by a transparent conductive oxide (TCO) layer. Typical TCO materials include zinc oxide (ZnO), tin oxide (SnO_2) and indium tin oxide (ITO). The TCO layers are an important cost factor in thin-film cell production. [42]

In the scientific literature the efficiency is often related to the aperture area (i.e. the photovoltaically active surface without edge and frame). Despite the relatively low efficiency, the energy yield can, under certain conditions, be quite considerable. The utilization of diffuse and low light is better with thin-film cells.

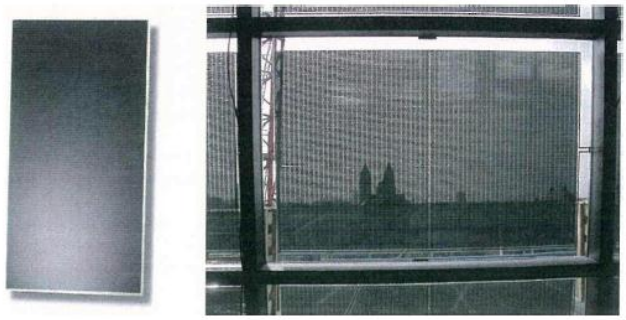

Fig.1.3: Typical strip appearance of a thin-film module, here made from CdTe (Source: First Solar)

In 1991, the first dye sensitized solar cell (DSSC) with a conversion of 7.1% was announced [12]. DSSC is a system, which mimics the photosynthesis in terms of transforming the solar energy to another form of energy, which is electricity. It is announced in 2005 that 11% efficiency is attained for a DSSC [13]. A typical DSSC achieved more than 10% sunlight to electrical power conversion efficiency [14] while 15-17% conversion efficiency has been attained by typical commercial silicon solar cell modules [15]. It may be noted that 1% efficiency is a typical value for tropical forest ecosystems [16] and 13% for the calculated limit for natural photosynthesis [17].

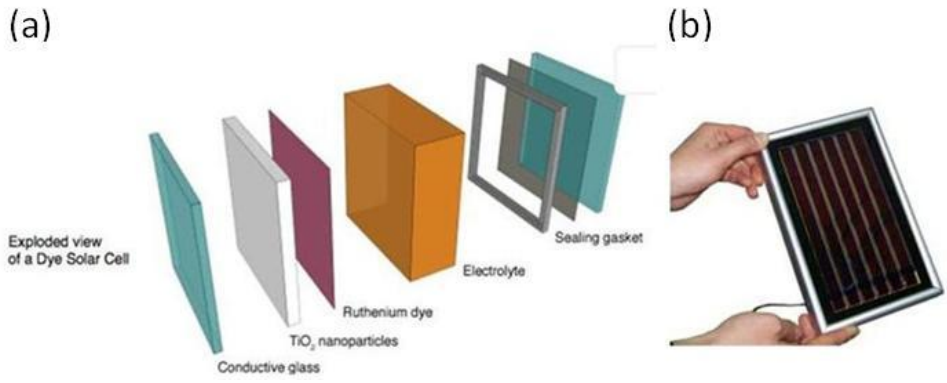

Fig 1.4: (a) Schematic Structure (b) Outlook of DSSCs [100]

Mainly, a typical DSSC is composed of a wide band gap oxide semiconductor, an electrolyte, a sensitizer (dye) and a counter electrode as it is shown in Figure 1.4. On the

anode side of the cell, dye is adsorbed on the semiconductor oxide, which is sintered on Transparent Conducting Oxide (TCO) glass. On the cathode side, there is another TCO with a catalyst coating over it. A redox electrolyte fills the gap between two TCO glasses. In general, semiconductor of choice is titanium dioxide, electrolyte couple is iodide/ triodide (I^-/I_3^-), counter electrode is platinum and the dye is the ruthenium based [26].

The dye-sensitized light-to-electron conversion process differs fundamentally from the one in the conventional solar cells. Figure 1.5 shows the energy band diagram of a p-n junction after thermal equilibration of charge carriers. The uncompensated charge caused by the diffusion of holes to the n region, and electrons to the p region, forms an electric field at the interface between the n and the p type semiconductor (space charge layer), which is characterized by the built in potential V_{bi}. Absorption of photons with an energy higher than the band gap results in the generation of excitons, which interact via columbic forces. Excitons recombine after a certain time under emission of photons or heat, unless they are separated by an electric field. Therefore, only excitons created in the space charge layer or close to it will contribute to the photocurrent.

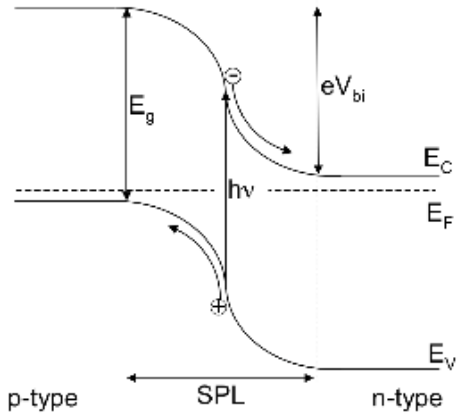

Fig 1.5: Energy band diagram of a conventional p-n junction solar cell under short circuit conditions [44]

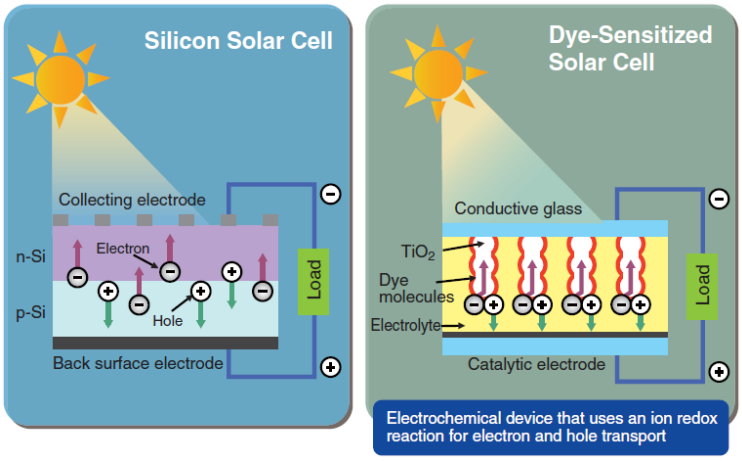

Fig 1.6: Difference between two types of cells [41]

Comparison of Figure 1.4 and Figure 1.5 demonstrates the difference between Dye sensitized solar cells and conventional solar cells:

1. Light absorption and charge carrier transport are separated in dye-sensitized solar cell, whereas both processes are established by the semiconductor in the conventional cell.

2. An electric field is necessary for charge separation in the p-n junction cell. Nanoparticles in the dye-sensitized solar cell are too small to sustain a build-in field; accordingly charge transport occurs mainly via diffusion.

3. Inside a p-n junction minority and majority charge carriers coexist in the same bulk volume. This makes conventional solar cells sensitive to bulk recombination and demands the absence of any recombination centers such as trace impurities. Dye-sensitized solar cells are majority charge carrier devices in which the electron transport occurs in the TiO_2 and the hole transport in the electrolyte. Recombination processes can therefore, only occur in form of surface recombination at the interface.

1.4 Comparison of solar cell types and trends

In most grid-connected solar systems, solar cells made from single-crystal and poly-crystal silicon are generally used. The lower efficiency of polycrystalline silicon is balanced out by a price advantage in manufacturing. Modules made from amorphous silicon have thus far been used predominantly in leisure applications (small appliances, camping and boats) and in architecture (facade systems and semi-transparent glazing).

Now that reservations concerning their stability and their ageing behavior have proven unfounded in new long-term test results, amorphous modules are currently enjoying a renaissance and are becoming increasingly established in larger systems. CIS modules have the highest efficiencies among the thin-film modules that have reached the mass-production stage; they are in use in various pilot projects.

As a cost-effective thin-film alternative, CdTe modules are already in use in megawatt-class ground-mounting systems. Highly efficient thin-film solar cells made from what are known as III-V semiconductors such as gallium arsenide (GaAs) or germanium (Ge), which comprise elements from Groups III and V in the periodic table, are not competitive in terms of price and are therefore, used only in space flight applications and concentrator systems, generally with additional III to V compounds such as GalnAs or GalnP. Efficiencies exceeding 30 % are, in principle, possible only with multi-layer cells. Hence, such Group III to V tandem and triple cells are interesting objects for research in the effort to set new world records for cell efficiency.

Among the organic solar cells, only dye-sensitized cells are currently market ready. These are an interesting and cost-effective alternative for the future. With their coloring and transparency they look set to create new accents, especially in building integration. The maximum values of the efficiency of solar cells and modules are summarized in Table 1. The average values for the modules available in the market are lower.

SOLAR CELL MATERIAL	CELL EFFICIENCY (Laboratory) %	CELL EFFICIENCY (Production) %	MODULE EFFICIENCY (Series Production) %
Monocrystalline silicon	24.7	21.5	16.9
Polycrystalline silicon	20.3	16.5	14.2
Crystalline thin film silicon	19.2	9.5	7.9
Amorphous silicon	13	10.5	7.5
Micromorphous silicon	12	10.7	9.1
CIS	19.5	14	11
Cadmium Telluride	16.5	10	9
III-V semiconductor	39	27.4	27
Dye sensitized solar cell	12	7	5
Hybrid solar cell	21	18.5	16.8

Table 1 - Maximum efficiencies in photovoltaic- Notes: (a) In a stabilized state, (b) Measured with concentrated irradiance. (c) Small production run. (Source: Fraunhofer ISE, University of Stuttgart, Ouaschning, Photon 2/2000)

Important drawbacks of the dye-sensitized solar cell are the volatility of the electrolyte and the corrosive action of the iodide redox couple. Correspondingly, long-term application of dye-sensitized solar cell is limited by the electrolyte permeability of the encapsulation and its inertness towards the iodine. A lot of effort is therefore, invested in finding less volatile electrolytes while maintaining sufficient hole transport. Approaches to replace the liquid electrolyte include application of ionic conducting polymer gels: [27-29] electrolyte gellated with amino-acid derivative [30] or room temperature molten salt [31]. Complete replacement of the liquid electrolyte system has been established using inorganic p-type semiconductors, such as CuI [32-36] or CuSCN [37, 38] as well as organic hole conductors, including low molecular weight charge transport materials [39] and semiconducting polymers [39, 40].

1.5 Solar cell Characterization

Intensity of the solar radiation depends on the distance between sun and earth and the distance varies between 1.47 x 10^8 km and 1.52 x 10^8km, the intensity changes between 1325 W/m^2 and 1412 W/m^2. Not all of the solar irradiation reaches the surface. The main reasons for decreasing the solar intensity are the reflection from atmosphere, adsorption by atmosphere, scattering by dust and pollutants in the air. During good weather conditions on an average 1000 W/m^2 solar intensity reaches the earth's surface at noon. Solar altitude spec is also important. When the altitude is perpendicular to the surface of the earth, solar radiation takes the shortest path to the surface and yields more energy; as the angle changes from 90°, path increases, which causes a decrease in energy reaching the surface. Thus, air mass (A.M.) factor is used to define the relationship between solar altitude height and A.M. For Europe, A.M. 1.5 is used as the average annual value [42].For instance, energy yield from the sun increases if the surfaces of the PV panels are always perpendicular to the sun [43].

The standard characterization techniques of DSSC include the determination of the DC current-voltage characteristic and analysis of the photocurrent-voltage curves includes determination of the following parameters:

- Short-circuit current (I_{SC}): Cell current measured at an applied potential of zero volt. I_{SC} is a function of the illumination intensity.
- Open-circuit potential (V_{OC}): Cell potential measured when current in the cell is zero, corresponding to almost flat valence and conduction bands.
- Maximal power output (P_{max}): For a given bias voltage the power output of the cell is the product of the measured cell current and the voltage P(V)=I·V. I_{max} and V_{max} are the coordinates of the maximum in the P(V) curve (maximum power point). The maximum power corresponds visually to the area of the largest rectangle, which can fit inside the current voltage curve.
- The fill factor (*FF*) is the ratio of the maximum power to the external short and open circuit values:

$$FF = \frac{I_{max} \cdot V_{max}}{I_{sc} \cdot V_{oc}}$$

This parameter indicates the deflection of the current-voltage characteristic from a square like curve is dependent on series and shunt resistance of the cell. Figure 1.7 illustrates the influence of increasing series resistance, R_s and decreasing shunt resistance, R_p on the current-voltage characteristic. To obtain high fill factors, R_s has to be as small as possible, while R_p needs to be as high as possible.

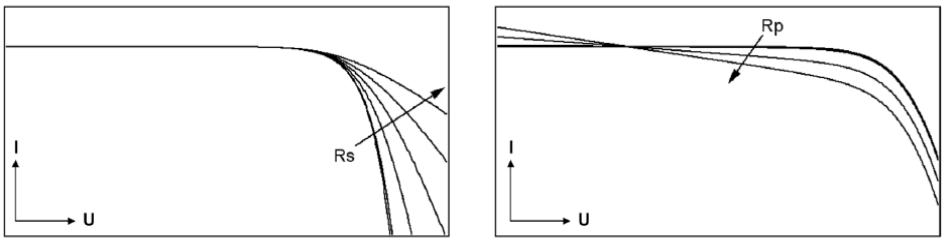

Fig 1.7: Illustration of the influence of increasing series resistance R_s and decreasing shunt resistance R_p on the I-V characteristic of DSSC [44]

- The efficiency **(η)** describes the performance of DSSC and is defined as the ratio of the maximum electric power extracted to the radiation power incident on the solar cell surface:

$$\eta = \frac{P_{max}}{P_{in}} = \frac{I_{sc} \cdot V_{oc} \cdot FF}{P_{in}}$$

The efficiency is a function of the V_{OC}, the I_{SC} and the FF of the cell. Accordingly, improvement of the photovoltaic yield is the result of the optimization of these three parameters.

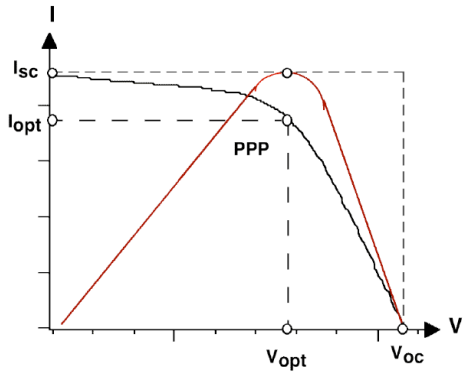

Fig 1.8: Illustration of Maximum Power Output from I-V Curve [44]

To compare solar cell characterized in different laboratories photovoltaic cells are measured under a set of standard test conditions such as the temperature of the cell should be 25°C and that the solar radiation incident on the cell should have a total power density of 1000 W/m^2, with a spectral power distribution characterized as AM1.5. The Air mass (AM) is the ratio of the path length of the sun's rays through the atmosphere when the sun is at a given angle Θ to the zenith, to the path length when the sun is at its zenith (Figure 1.9). This relation can be approximated by:

$$AM = 1 / \cos \Theta$$

An Air Mass distribution of 1.5, as specified in the standard test conditions, corresponds to the spectral power distribution observed when the sun's radiation is coming from overhead angle of about 48° [44].

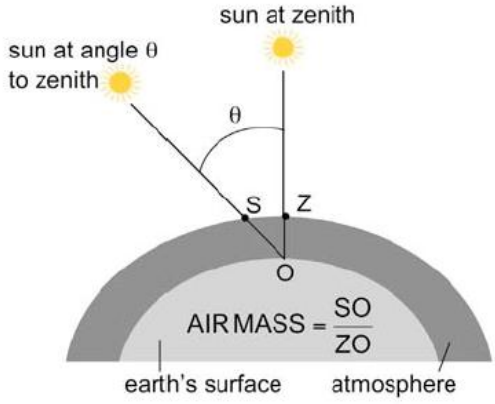

Fig 1.9: Illustration of Air mass concept [44]

2. LITERATURE SURVEY

2.1 History of Photo electrochemical and DSSC Cells

The energy demand of the world increases each year, the importance of the renewable energy sources like solar energy increases more and more each day especially for the countries in the solar rich region. Many solar cell products are already in the market and new ones like DSSC are coming. DSSC is a new type of solar cell that mimics the photosynthesis. It is much cheaper than conventional solar cells and its production is simpler than photo-voltaics.

Becquerel completed photoelectric experiments in 1839 using a metal halide salt to produce current between two platinum electrodes, which were immersed in the electrolyte by the motivation of photography. Then the first photographic images were made by Daguerre in 1837, following the silver halide process by Fox Talbot in 1839. However, these films were found to be particularly insensitive for wavelengths greater than 460 nm of the electromagnetic spectrum due to wider band gap (2.7-3.2 eV) and blocked absorption of light [45]. Vogel's discovery in 1883 realized that adding a dye to the silver halide emulsions made it possible to extend the photosensitivity of silver halide emulsions to longer wavelengths [46]. In 1887, Moser demonstrated the concept of dye on silver halide electrodes of photo electrochemical cells and came as a surprise to many chemists [47]. The cyanine and the combination of two cyanine dyes were particularly effective for photo electrochemical processes and recognized by Namba and Hishiki in 1964 [48]. Then, the concept of adding dyes on the semiconductor electrodes to enhance efficiency of the photo electrochemical cell became a common consensus. Brattain and Garret lead the modern photo electrochemistry towards a thriving research direction. Gerischer was the first one to study the semiconductor–electrolyte interface of the photo electrochemical cells [49-50]. After the oil crisis in 1973, huge number of publications on photo electrochemical cells appeared based on a worldwide quest for alternative energy sources.

According to Gratzel, the first sensitization of a photo electrode followed immediately after the rendering of a black and white image in the 1870s [51]. However, the realization that the two procedures work similarly through the injection of electrons from photo excited dye molecules into the conduction band of the n-type semiconductor substrate didn't occur until 1960s. In subsequent years, the idea developed that the dye could function most efficiently if it is chemisorbed on the surface of the semiconductor. The concept of using dispersed particles to provide a sufficient interface emerged, and then photo-electrodes were employed [51].

TiO_2 became the semiconductor of choice due to its many advantages for sensitized photochemistry and photo-electrochemistry. TiO_2 is a low cost, non-toxic, widely available and biocompatible material. The standard dye until that time was tris (2, 2 bipyridyl-4, 4 carboxylate) Ruthenium (II), the function of the carboxylate being the attachment by chemisorption of the chromophore to the oxide substrate. Progress thereafter, was incremental and was a synergy of structure, substrate roughness, morphology, dye photo physics and electrolyte redox chemistry. The extensive research led to formation of the sensitized electrochemical photovoltaic device in 1991 with conversion efficiency (at that time) of 7.1% under solar illumination. This evolution of more efficient DSSC has continued progressively since then, with certified efficiency now over 10%.

2.2 Operating Principle of DSSC

A typical DSSC is composed of a wide band gap oxide semiconductor, an electrolyte, a sensitizer (dye) and a counter electrode as it is shown in Figure 2.1. On the anode side of the cell, dye is adsorbed on the semiconductor oxide, which is sintered on Transparent Conducting Oxide (TCO) glass. On the cathode side, there is another TCO with a catalyst coating over it. A redox electrolyte fills the gap between two TCO glasses. In general, semiconductor of choice is titanium dioxide, electrolyte couple is iodide/triodide (I^-/I_3^-), counter electrode is platinum and the dye is the ruthenium base one [53]. The working principle of a DSSC begins with the photo excitation of sensitizer

by adsorption of incident solar radiation. After the sensitizer is excited, it injects its electron to the conduction band of the oxide, which is anchored to the sensitizer. Then, the electron from electrolyte regenerates excited sensitizer, which is a redox couple, typically iodide/triodide in an organic solvent. The oxidized dye is regenerated by taking electron from the iodide and forming triiodide. The iodide is further regenerated by the triiodide at the counter-electrode. Cycle is completed by the electron migration between TiO_2 (anatase) and counter-electrode, which is usually Pt coated TCO. The electron cycle of the system is showed in Figure 2.1 [52, 54].

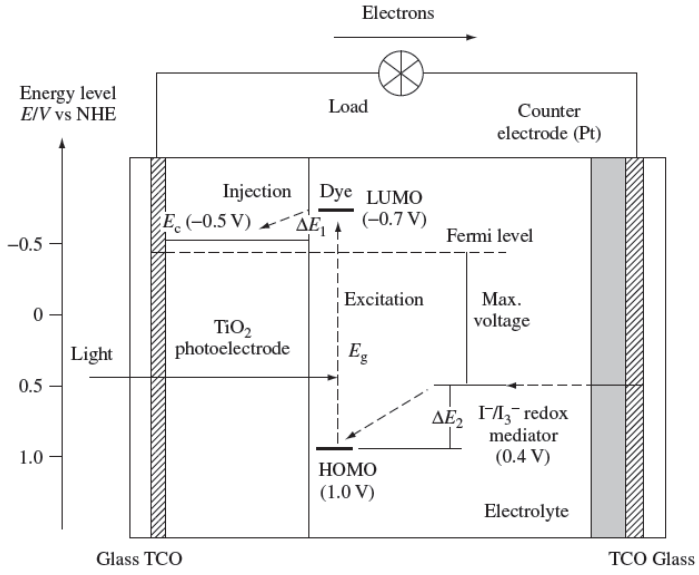

Fig 2.1: Operating principle of DSSC [51]

The electron cycle in the cell was studied by Gratzel, 2001 [55] and is given in Figure 2.2:

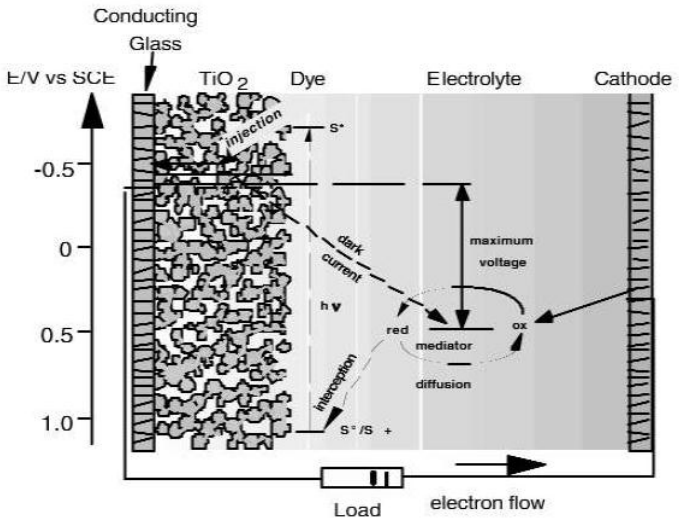

Fig 2.2: Electron cycle in the DSSC [55]

For harvesting the solar energy, a sensitizer is adsorbed on a semiconductor oxide as mentioned before. However, a monolayer of dye can absorb very limited amount of solar energy due to the limited cross section area of the dye molecules. Also, multilayer application of dye is not a solution because the layers filter the solar rays. Thus, another strategy is used to increase the light capture cross section. Mesoporous nano size TiO_2 is used to increase the total surface area. It is emphasized that, the dye covered nano-oxide sponge absorbs solar rays much better due to increase of the surface area; achieved by introducing the nano particles. The semiconductor oxide surface increases by 1000 times for a 10 μm mesoporous nano-oxide film, which means that the efficiency to capture the sunlight by dye covered oxide enhances significantly [55].

There are two main regeneration phase systems in a DSSC, which are solid state DSSC and liquid state DSSC. DSSC using a liquid electrolyte includes a redox couple to regenerate the sensitizer. Electrolyte is composed of an organic solvent and a I-/I3- redox couple. Ion in the electrolyte regenerates photo excited dye molecule. Voltage produced by DSSC is the difference between the chemical potential of the titanium dioxide (Fermi level) and the redox potential of the electrolyte. Generally, KI or LiI and I_2

are dissolved in an organic solvent, usually acetonitrile (ACN) or ethylene glycol. The main reactions proceeding in the system are described by Smestad [56] and also by Hauch and George [53] and they are given by the equations from (1-1) to (1-4).

Dye molecule is photo excited by the equation:

$$Dye + light \rightarrow Dye^* \quad \text{..... (1-1)}$$

Then, it ejects its electron to the conduction band of the semiconductor oxide as it is shown in equation (1-2).

$$Dye^* + TiO_2 \rightarrow e^- (TiO_2) + Dye^+ \quad \text{..... (1-2)}$$

Dye molecule is reduced by the electrolyte couple with the reaction given below:

$$2\ Dye^+ + 3\ I^- \rightarrow I_3^- + 2\ Dye \quad \text{..... (1-3)}$$

Then, at the cathode side of the cell, which is usually Pt, iodide is regenerated by taking the electron.

$$I_3^- + 2\ e^- \rightarrow 3\ I^- \quad \text{..... (1-4)}$$

Surely the charge transfer resistance of Pt and diffusion constant of triiodide are also important parameters for the regeneration process [53, 56]. Counter electrode or cathode, is used to regenerate the electrolyte couple which, in turn, regenerates the photo excited dye molecule. In other words, counter electrode is responsible for catalytic cathodic reduction of triiodide to iodide. Although many other materials like carbon and conductive polymer are tried, platinum is still the most preferred material because it shows high catalytic activity for triiodide / iodide reduction and its light reflectivity is at an acceptable amount. Many platinum coating techniques are used like electron beam evaporation, sputtering, thermal decomposition, electro deposition and thermal treatment for platinization of the cathode.

The efficiency of a DSSC strictly depends on the sensitizer. Following properties for a sensitizer are quite important. Absorption spectrum of the dye is critical because dye should adsorb the visible light. Also, the redox properties of the ground state and excited state of the dye molecule have to be examined. Because both electron transfer between

sensitizer and electrolyte and between sensitizer and TiO_2 strictly depends on this criteria. Besides, anchoring ability of dye to the TiO_2 affects the electron transfer. Energy levels of the dye and semiconductor oxide must be suitable such that electron can be transferred from dye molecule to the semiconductor oxide as it is described in Figure 2.2.

Carboxyl or hydroxamate groups can anchor the dye molecules to TiO_2 well so electron transfer from dye molecule to the conduction band of TiO_2 molecule can be made successfully. In addition to these, dye should be regenerated fast enough after losing its electron. Finally, it should be stable for 20 years of exposure to natural light for being economically feasible [14]. According to the criteria given above, Ru and Os based sensitizers are the best molecules reported up to now. General structure of a typical sensitizer is ML2(X) 2, where L 2, 2'-bipyidyl-4, 4'-dicarboxylic acid, M is Ru or Os and X is halide like cyanide, thiocyanate or water. Note that most famous dye N3 was found in 1993 and ruthenium complex of it is cis-RuL2-$(NCS)_2$. Black dye that adsorbs the near-IR appears to be better than N3 [55, 57, 58].

2.3 Characteristics of DSSC

The DSSC has the following unique characteristics such as the following:

- High energy conversion efficiency: A DSSC efficiency is equal to that of the amorphous Silicon (a-Si) solar cell that was obtained in a laboratory setting and efficiencies greater than 11% is desired.
- Low-cost fabrication: The DSSC is very simple to construct using low-cost materials. Fabrication costs will therefore, be less than that for conventional solar cells. For example, the US $0.60/W, which may be competitive for conventional solar cells, has been estimated for a DSSC with 10% efficiency.
- Abundant supply of component materials: Oxide semiconductors such as TiO_2, dye, and iodine are abundantly available. Although metal deposits of Ru are limited, the amount of Ru complex used in the DSSC is only 1×10^{-7} mol cm^{-2}. Organic dye photosensitizers could be used rather than Ru complexes if resource limitation is a problem.

- Good potential for colorful, adaptable consumer products: Colorful and transparent solar cells can be made using various kinds of dyes, depending on the use of the cell. For example, transparent solar cells could be used in place of windowpanes. Additionally, the use of a plastic substrate, rather than glass, is possible if low temperature processing of the TiO_2 film preparation (<250°C) is available and would expand the use of DSSC.
- Low potential for environmental pollution: The TiO_2, dyes, and iodine used in the DSSC are nontoxic. The only component that could potentially cause harm is the organic solvents used in the electrolyte solution. Future research should be directed toward developing a solid-state electrolyte.
- Good recyclability: The organic dye photosensitizers adsorbed on the electrode can be removed by washing the electrode with alkali solutions or combustion, providing recyclability of the DSSC.

2.4 Equivalent circuits of DSSCs

The mechanism of conventional solar cells is well understood by way of equivalent circuits. Equivalent circuits are very useful to analyze devices and improve performance. Understanding of the DSSC's equivalent circuit is essential to improve the development of new DSSC based photovoltaic modules. Electrochemical impedance spectroscopy (EIS) is used to analyze the DSSC's internal resistance. Conventional solar cells have well established equivalent circuit models. Since DSSCs does not have established and standard fabrication process, it does not have standardized models. Figure 2.3 shows an electrochemical impedance spectrum of the DSSC using N3 dye. The figure shows that there are three impedances in the DSSC. Three semicircles are observed in the measured frequency range of 20−1 MHz.

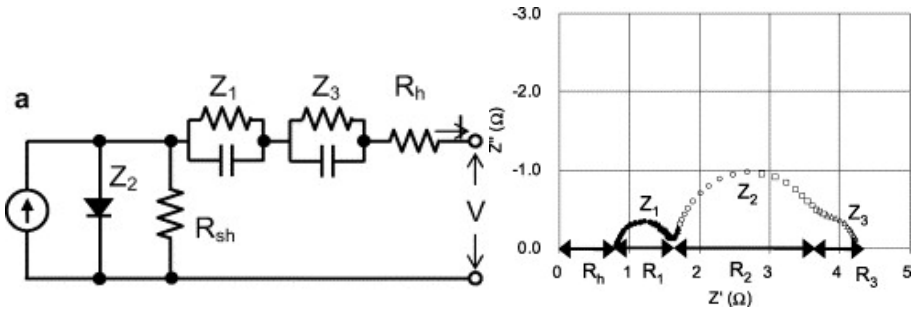

Fig 2.3: (a) Equivalent circuit of DSSC (b) Example of Nyquist plot [122]

The impedances between 100 and 1 kHz as Z_1, 1 kHz to 1 Hz as Z_2, 1 Hz to 20 MHz as Z_3. The internal resistances R_1, R_2, and R_3 describe the real parts of Z_1, Z_2 and Z_3, respectively. Since impedance over 1 MHz was not measured due to instrument limitations, the resistance element in this frequency region was defined as R_h.

R_h, which locates high frequency range > 106 Hz frequency area, represents the sheet resistance of the TCO substrate and is primarily influenced by the thickness of the conductive layer on the electrode. R_1 is related to the carrier transport resistance at the surface of Pt counter electrode and can be varied changing the roughness factor of counter electrode. Changing the distance between TCO and Pt counter electrode can optimize R3, which represents the diffusion of iodide and triiodide within the electrolyte. R2 shows the resistance of the diode element in the DSSCs, and reflects the properties of the photo-injected electrons within the TiO_2. The series internal resistance, Rs, is defined as the sum of the resistance R_1, R_3, and R_h. The variation of each resistance identifies a different direction to optimize the DSSCs efficiency.

Many equivalent circuit models were proposed to explain DSSCs. Warburg element associated with the diffusion in the electrolyte [59]. A standard Randles equivalent circuit depicted the equivalent circuit of DSSCs by R_S (TCO series resistance), R_{ct} (sum of the charge-transfer resistances of both electrodes), and Z_d (diffusion impedance) [60].

2.5 Semiconductor Oxide in DSSC

Semiconductor oxide is mainly prepared using the Sol-Gel procedure and the advantage of this procedure is that it is quite easy to adjust the particle size, nanostructure and porosity of mesoporous nano-oxide film. Process is strictly temperature dependent. However, we make use of semiconductor oxide (TiO_2) commercially prepared from Solaronix. In most Sol Gel procedures the resulting TiO_2 particles are in the form of anatase or rutile according to the parameters used in sol-gel procedure. A standard sol is treated for about 450 °C to establish a strong contact between the particles and it is reported that resulting film thickness is typically 5-20 μm and TiO_2 mass is about 1-4 mg/cm^2, porosity is 50-65 % [67, 68].

It is known that choosing the right semiconductor is an important step in the process and some requirements must be satisfied by the semiconductor. For instance, mesoporous sponge structured oxide films are needed to be n-doped to conduct electrons and it has to be a wide band gap oxide. Many materials like TiO_2, ZnO, SnO_2 and Nb_2O_5 are the wide band gap oxides and have been investigated for years but TiO_2 (anatase) became the semiconductor of choice because it meets all requirements. Moreover, it is cheap, non-toxic and easy to produce [70]. Additional studies are conducted on semiconductors, which are doped with other metals to increase the efficiency. For instance, Keis et al. found that a higher efficiency is obtained for Al-doped ZnO films compared with the undoped ones. It is stated that Al doping process generated more free electrons, consequently produced better conductivity to increase the efficiency [69].

The optical enhancement studies have been performed focusing on increasing the light capture capabilities of the DSSC. For example, titania inverse opals are covered on the nanocrystalline TiO_2 layer such that it forms a bilayer of semiconductor oxide. A polymer film is used to prevent filling of titania inverse opals into the mesoporous structure of nanocrystalline TiO_2. Lee et al. published that addition of titania inverse opals to nanocrystaline TiO_2 layer increased the efficiency from 6.5 to 8.3 % under the anode

side illumination [71]. There are many studies conducted in the literature for making the TiO_2 deposition applicable for mass production. For instance, sputtering process is thought to be one of the best candidates for mass production. Magnusson et al. obtained 2.34 mA/cm^2 short circuit current density for 9.7 μm film thickness prepared by sputtering instead of sol-gel procedure. Also they attained maximum open current voltage value of 0.4-0.6 V. Moreover, it is stated that a higher short circuit current value is attained for sputtered deposition than the sol-gel prepared film for the same TiO_2 thickness [72].

2.6 Sensitizer

Sensitizers are the chemicals, which are used to absorb the visible light and inject their electron to the semiconductor oxide to start the electron transport cycle in the cell. Most typically, Ru based dyes are preferred as sensitizers. For instance, the standard dye is tris (2, 2'- bipyridyl, 4, 4'-carboxylate) ruthenium (II) was used by Grätzel and his co-workers in 1991 [73]. There are many studies on sensitizers to increase the efficiency of the DSSC. For instance, a cis - dithiocyanato bis (4,4A - bicarboxy - 2, 2 A – pyridine) ruthenium (ii) complex gives a solar to electric power conversion efficiency of 10% at AM 1.5 condition. For improving the efficiency, sensitizer has to be more sensitive to red and near-IR region of the light. Nazeeruddin et al. announced that a black trithiocyanato–ruthenium (ii) terpyridyl complex where the terpyridyl ligand is substituted by three carboxyl groups is very efficient over the whole visible range and gives good response to the near-IR region up to 920 nm [74]. Besides, boradiazaindacenes (BODIPY) based dye is studied as sensitizer because these molecules are useful fluorescent labels for biomolecules. Ela et al. observed that BODIPY system gives 1.66% efficiency, 4.03 mA/cm^2 short circuit current and 0.562 V open circuit voltage [75]. Even though Ru based dyes are the most preferred ones because, they provide the highest efficiencies, and it is hard to synthesize them. It is also possible to use some kind of natural fresh fruits like raw berries and strawberries as sensitizers but their efficiencies are quite low and these dyes still require further purification processes. There are some

studies on natural dyes such as chlorophyll derivatives studied by Kay et.al [76] and observed on the average 2.6% efficiency and current of 9.4 mA/cm^2.

Successive absorption of the light in a wavelength range from visible to IR is quite important to increase the efficiency of the cell. To achieve this feature, not only new sensitizers having larger absorption ranges are developed but also co-sensitization of dyes are used at the same time such that one dye absorbs blue part of the visible spectrum and the other adsorbs the red part and near IR spectrum.

The aim of using different dyes in the same DSSC is to increase the efficiency by making the DSSC compatible with a wider light spectrum. For example, Kuang et al. reported that the co-sensitization of dyes yields 6.4% efficiency under A.M. 1.5 sunlight [77]. The best photovoltaic performance has so far been achieved with polypyridyl complexes of ruthenium and osmium. Sensitizers having the general structure $ML_2(X)_2$, where L stands for 2,2-bipyridyl-4,4-dicarboxylic acid M is Ru or Os and X presents a halide, cyanide, thiocyanate, acetyl acetonate, thiacarbamate or water substituent, are particularly promising. The ruthenium complex cis-$RuL_2(NCS)_2$, as shown in the Figure 2.4, known as N719 dye has become widely used sensitizer for mesoporous solar cells. The fully protonated N719 has absorption maxima at 518 and 380 nm and the complex emits at 750 nm with the 60ns lifetime.

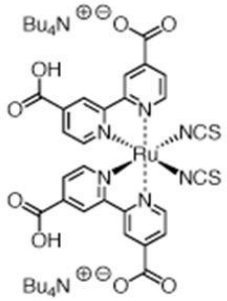

Fig 2.4: Chemical Structure of Ruthenium N719 dye

2.7 Electrolyte

Many redox couples are studied to find the most suitable electrolyte system for DSSC. For instance, potassium iodide was mixed with iodine in water-free ethylene

glycol by Smestad [78]. A few drops of electrolyte were added to edge of the DSSC and it was soaked by capillary force. In another study conducted by Hauch and George, DSSC was filled with the electrolyte of lithium iodide and iodine in acetonitrile [79]. Besides the studies on the redox couples, some studies for decreasing the loss of electrolyte in the DSSC were also conducted. For instance, the electrolyte may leak because many sealing difficulties could be encountered during assembly, solid state DSSC was developed to eliminate the sealing problem.

In a typical DSSC, electrolyte can leak or evaporate with time. Another solution rather than using solid state DSSC is using an electrolyte having a higher viscosity to decrease the rate of leakage. For instance, viscosity of typical ionic liquids is about 100 times greater than that of acetonitrile, which is a typical organic solvent in DSSC. The main advantages of ionic liquids are non- volatility, non-flammability and high ionic conductivity. Kawana et.al prepared a DSSC having EMImDCA as ionic liquid and announced an efficiency 5.5% under 1000 W/m^2 light intensity [80].

Also, there are studies on the electron transport kinetics. For example, Peter et al. stated that in an efficient cell, back transfer of electrons, which are resulted from photo injection, has to be as slow as possible such that electrons can accumulate in the oxide and generate voltage. However, regeneration process at the cathode side must be fast enough to prevent production of a large over potential loss when the current flows [81].

2.8 Counter electrode

2.8.1 Platinum Coated Counter Electrode

The counter electrode is ideally a high conductivity material and exhibits an ohmic contact to the hole conductor, which requires work function matching of hole conductor and counter electrode. It is constituted by a glass coated transparent film deposited with a platinum layer. When a photon excites the dye molecule, it injects electrons into the semiconductor layer. A redox reaction in the electrolyte ($3I^- \rightarrow I_3^- + 2e^-$) provides the electron back to the dye molecule. The triiodide in turn accepts electrons, and is reduced to iodine ($I_3^- + 2e^- \rightarrow 3I^-$) to regenerate the redox couple. The

efficiency of a DSSC is based on different rate constants for iodine reduction between the working and counter electrodes. The iodine reduction at the counter electrode has to be several orders of magnitude faster than the recombination at the TiO_2/electrolyte interface. The regeneration of the oxidized dye occurs in the nanosecond range, which is typically 100 times faster than any recombination reaction and about 10^8 times faster than the intrinsic lifetime of the oxidized dye.

2.9 Synthesis of CNTs for DSSCs Application

2.9.1 Characteristics of CNTs

In 1985, the C60 fullerenes were discovered by Professors Richard E. Smalley and Robert F. Curl of Rice University and Professor Harold Kroto of the University of Sussex in Brighton, England [62]. Later, carbon nanotubes (CNTs), which form the fourth allotrope of carbon, were found in their multiwall form by Iijima in 1991 [63]. CNTs are the allotropes of carbon with a long, thin cylindrical nanostructure and are held together by Van der Waals forces. CNTs have attracted several researchers because of its remarkable structural, mechanical, electrical, and thermal properties. The electrical conductivities of CNTs are around 10^9 $A.cm^{-2}$, which are 10^7 times higher than that of the copper [64-65]. From the mechanical point of view, CNTs are expected to be the ultimate high-strength fibers by their enduring bonds. MWCNTs have a high tensile strength of about 63 GPa and make them suitable for incorporating them into high technical devices, such as probe tips [66]. CNTs can be defined as single-walled carbon nanotubes (SWCNTs), double-walled carbon nanotubes (DWCNTs) and multi-walled carbon nanotubes (MWCNTs) based on the arrangement of their graphitic sheets. The properties of CNTs make them suitable for nanotechnology, electronics, optics, material science, architecture etc. In alternative energy technologies, CNTs are used based on their high conductive and mechanical properties. Figure 2.5 depicts the physical structure of MWCNT and SWCNT.

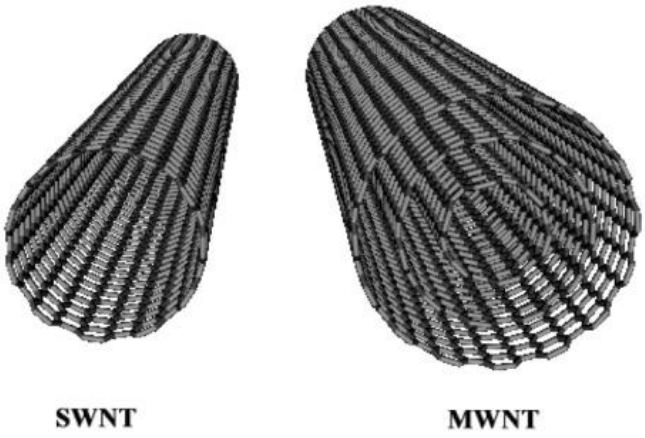

Fig 2.5 Molecular structures of a single-walled carbon nanotube (SWNT) and of a multi-walled carbon nanotube (MWNT)[61]

SWNTs could potentially be used in several of the research and development areas directed toward composite structural and electronic materials. Covalent functionalization of SWNTs has given scientists and engineers the ability to manipulate these astonishing structures in ways that would otherwise be unattainable [89,90]. SWNTs consist of only carbon and can be considered theoretically as a graphene sheet rolled into a seamless cylinder [91, 92]. SWNTs, the strongest material known, are ladder polymers; i.e., more than one bond needs to be broken to cleave the backbone. Typical ladder polymers are fully joined by only two repeating bonds. However, depending on the tube type, SWNTs have 10 to 20 carbon–carbon bonds per repeat unit that would need to be broken for polymer strand rupture to occur. Furthermore, each of those 10 to 20 carbon–carbon bonds has a bond order of ca. 1.3, and since the carbon–carbon bond is among the strongest bonds, it is unlikely that we will ever find more robust polymeric chains. Beyond their amazing mechanical properties, they also exhibit extraordinary optical, electrical, and thermal properties[93], as nanotubes can be either carbon-based metals or semiconductors[94,95] and have been used in the construction of nanotube-based transistors,[90,96] as well as serving as interconnects in a small integrated circuit [97]. Furthermore, nanotube-based composites show tremendous promise; the

lightweight yet strong, flexible,[98] and resilient [99] nanotubes can add fortification to many polymeric structural materials. Unfortunately, much of the optical, electrical, and thermal properties are extended pi-conjugation dependent, and therefore, covalent functionalization causes a loss in these qualities.

2.9.2 Synthesis of CNTs

Due to CNTs' unique structure, the interaction between the matrix and the reinforcement is hard to breakthrough. Only few concentrated acids are able to break the bonds between carbon atoms. In addition, its uncontrolled agglomeration due to the nanometer size also blocks the commercialization. One of the remedies to increase the interaction between matrix and reinforcement is to functionalize CNTs by inserting functional groups on the sidewall of CNTs [82]. Sulfuric acid (H_2SO_4) and nitric acid (HNO_3) are common acids used to insert carboxyl groups (-COOH) on the surface of CNTs [83-85]. Some scientists also added hydrochloric acid (HCl) to insert functional groups on the CNTs successfully [86]. In addition, other combinations of acids were researched to insert functional groups on the CNTs. Xie *et al.* used a mixture of H_2SO_4/HNO_3 (3:1) and H_2O_2 to obtain carboxyl and hydroxyl groups [87]. H_2O_2 can also be used alone to obtain carboxyl groups [88].

2.9.3 Synthesis of SWCNT- TiO_2

SWCNTs considered as suitable materials to enhance efficiencies of the DSSCs based on their high conductivity. The TiO_2 layer and the counter electrode in the DSSC are the places to incorporate SWCNTs, which helps in reducing the internal resistances of the cell. There are several methods to synthesize the SWCNT-TiO_2 layer in DSSCs. The cost-effective method: direct mixing method, was proved to enhance the efficiency of DSSCs by a factor of two. The influence of single-walled carbon nanotube (SWCNT) architectures for facilitating charge transport in mesoscopic semiconductor films has been probed. The dye-sensitized solar cells constructed using this SWCNT scaffold or support structure show an improvement in the photocurrent generation. However, this improvement in photocurrent generation is neutralized by a lower photo voltage as the

apparent Fermi level of the TiO_2 and SWCNT composite becomes more positive than that of pristine TiO_2.

Semiconductor nanotube or nanowire assemblies, when assembled on the electrode surface and then modified with dye molecules, offer the possibility to improve the charge collection and transport of charge carriers. Such one-dimensional nanostructures have recently been shown to direct the flow of photo generated charge carriers in DSSCs [101-106] and quantum dot solar cells [107,108]. Another approach involves the use of a SWCNT network on a conducting electrode surface to promote charge transport in mesoscopic TiO_2 films. The electrons injected from the excited dye into TiO_2 nanoparticles are then transferred through a SWCNT scaffold to generate photocurrent. The semiconducting property of SWCNT has been successfully exploited to improve the performance of organic photovoltaic cells and fuel cells [109,110]. By employment of a SWCNT network as a conducting scaffold, we can achieve 2-fold enhancement in the photocurrent generation of the TiO_2 particulate films [111,112]. The organization of photoactive donor acceptor assemblies (e.g., porphyrin and C60) on the electrode surface has already been shown to offer significant enhancement in the photo conversion efficiency of solar cells [113-116].

The SWCNT-TiO_2 layer formed by electrophoretic deposition can also be used as it helps in preventing the micro cracks by strengthening the bonding between the TiO_2 particles and SWCNT support structure. Some research groups followed the same concept to enhance the efficiency of DSSCs using well-aligned TiO_2 nanotubes and the TiO_2 -nanowires [117-118].

3. METHODOLOGY AND EXPERIMENTAL PROCEDURE

3.1 Experimental Methods

The photo conversion efficiency of DSSC is significantly dependent on the uniformity and quality of electrodes; hence in previous work of our research group we have optimized the thickness of TiO_2 film and nanoparticles' size in the film. One more important aspect of the research was to improvise the fabrication process and design. The research work carried out in this project explores different ways and methods to improve the semi-automated fabrication process. The different parameters involved in the process were assessed for their tolerances and their considerable variation from the control limits. The parameter with the highest variation was modified in the fabrication process and the data was collected to compare and track the improvement in the efficiency of cells. Additionally, the work presented in this paper appraises performance improvements in Dye sensitized solar cell by changing the platinum coating process of the counter electrode. The coating process for the platinum counter electrode was changed from the standard doctor blade coating to sputtering platinum on the counter electrode. The cells were fabricated with this configuration of the cell and the data was collected to measure and compare the efficiencies of cells between two different coating processes. . The second phase of the work focused on incorporation of SWCNT into the TiO_2 electrode and its effect on the cell efficiency. Following content describes the fabrication process in detail as well as the changes made to the previous version of the process, which forms the methodology.

3.2 Fabrication procedure of DSSC

The most critical part in DSSC is the fabrication process. The uniformity and repeatability in the fabrication procedure is critical and deterministic for getting good and efficient results.

Figure below gives is a snapshot of the different fabrication steps adopted.

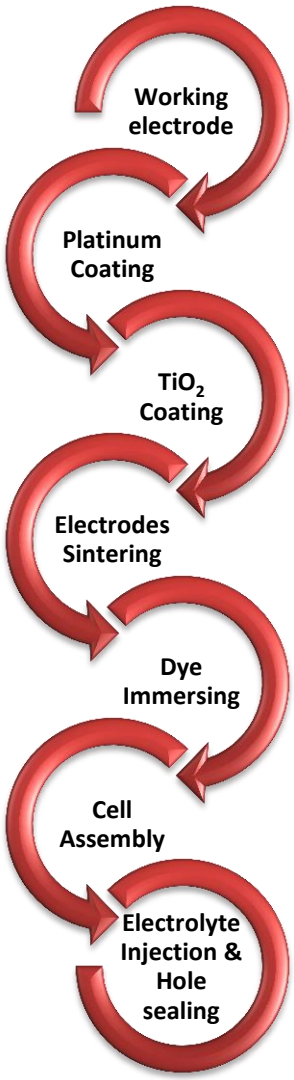

Fig 3.1: Dye sensitized solar cell fabrication process

3.2.1 Preparation of Transparent conductive oxide glass electrode

The first step is to cut the tin coated glass electrode to fabricate a finished cell size of 0.5 cm X 0.5 cm. The two electrodes for the cell are prepared by cutting the conductive electrode material into sizes of 1.25 cm x 1.25 cm. The electrode size has huge influence on the efficiency of the cell as the sheet resistance of the conductive glass electrode reduces the efficiency of the cell. Therefore, smaller electrode sizes were preferred for fabrication of the DSSC. These cut electrodes were then rinsed with

isopropyl alcohol (IPA) to remove the surface impurities like small glass particles arising from the cutting of the glass electrode.

Further, preparation of the counter glass electrodes, a small hole is drilled in the middle of the glass electrode using a 1 mm drill bit to accommodate the electrolyte injection process after cell assembly. Cutting of glass electrodes and hole drilling operations were done with utmost care in order to ensure that the conductive surfaces of the electrode are protected during the process. Rinsing of cut glass electrodes was repeated to remove surface impurities.

Fig 3.2: Laser Machine (Universal laser system) used for cutting glasses and making the coating cross sections

3.2.2 TiO_2 coating on working electrode

The main requirement of the fabrication process was to make it repeatable and reproducible. The uniformity of TiO_2 is very essential for making an efficient cell. The Coatema tool was introduced in the coating process to improve the uniformity. Besides, the glass rod was attached to the Coatema tool to make the process more automated to avoid variations arising from human intervention during the coating of the TiO_2 film on the working electrode. Following information enumerates the process of coating TiO_2 on the working electrode.

TiO_2 coating step forms the most important step in the fabrication as the quality of the thin film determines the performance of dye sensitized solar cell. The Coatema tool

was used for the screen printing of the TiO_2 layer on the glass electrode. In the beginning, the Coatema tool was calibrated in terms of pressure and the level of glass rod so that coating is done along the substrate.

Fig 3.3: Coatema tool

Prior to coating, TiO_2 paste (Ti-Nanoxide-20 D, 20 nm, Solaronix) was sonicated for about 5 minutes to eliminate the aggregation of TiO_2 particles. The desired thickness of TiO_2 layer was first determined using different layers of 3M Magic Tape (~100µm) on the PVC mask while a 0.6 cm x 0.6 cm area on the tape was cut by the laser machine. The working electrode was attached underneath the tape and was placed on the metallic plate of the Coatema tool to carry out the TiO_2 coating.

Fig 3.4: Sonication of TiO_2 paste and cell area definition on substrate using scotch tape

TiO_2 coated FTO glass electrode was dried for 1 hour with the petri dish covered on top to avoid the dust particles and also to reduce the irregularity of the surface before sintering process.

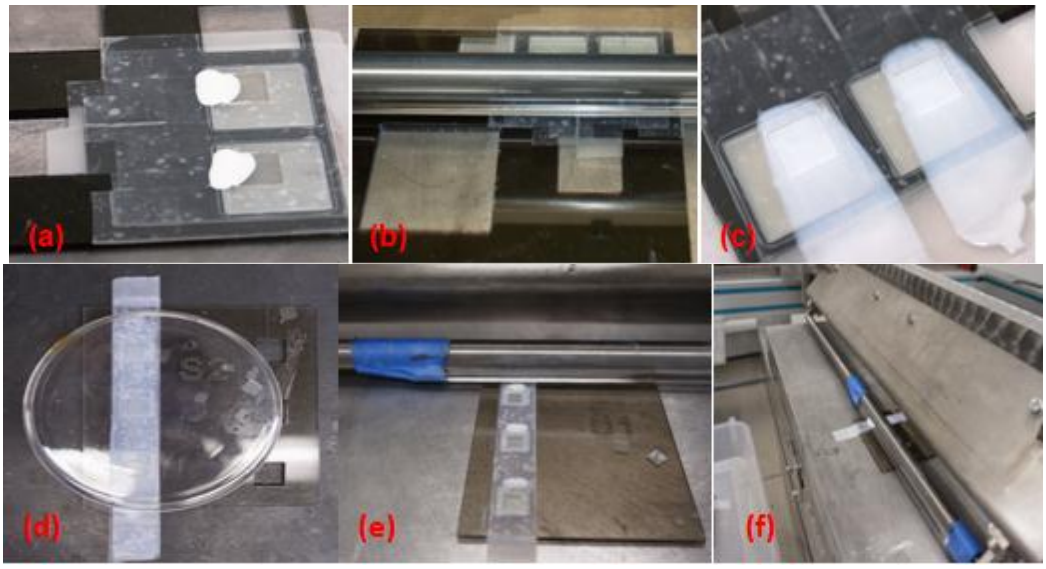

Figure 3.5: (a) Working electrodes prior to TiO_2 coating (b) TiO_2 coating with Coatema tool (c) TiO_2 coated electrodes (d) Drying of electrodes (e) Substrate coating procedure (f) Coating procedure (Angular view)

3.2.3 Platinum coating on counter electrode

A platinum layer (Platisol Figure 3.6 (a), Solaronix), which acted as a catalyst, was deposited on the counter electrode to reduce over potentials of the iodide/tri-iodide redox couple. The fabrication procedure is same as of the TiO_2 layer. Two layers of 3M Magic Tape was used to define a 0.25 cm x 0.25 cm cell area. The eyedropper was used to apply the platinum solution onto the counter electrode. The counter electrode had a hole to inject the electrolyte to complete the DSS cell assembly; however, these holes were sealed during platinum dipping. After curing the platinum coated counter electrode inside a vacuum chamber with cover overnight at room temperature, the counter electrode was dried at 400° C for one hour. A quasi-transparent activated platinum layer Figure 3.6 (b) was observed on the surface of the counter electrode.

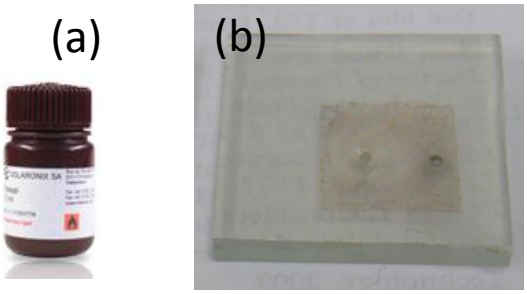

Fig 3.6: (a) Platisol (b) Platinum coated Counter Electrode

An alternative method for the platinum coating on the counter electrode tried in this work was the sputtering process. Many literature articles have suggested the alternative of sputtering platinum on the counter electrode. This alternative platinum coating on the counter electrode process forms the integral part of the thesis.

3.2.4 Electrodes Sintering

Once the working electrode and counter electrode were coated with TiO_2 and platinum respectively, both electrodes were removed from the PVC mask and were kept in separate Petri dishes. They were then sintered in the furnace at 400 °C for one hour and forty five minutes. The time period for sintering process was determined by carrying out different experiments with time as a parameter. Both electrodes were kept in the furnace over night while the furnace cooled down to room temperature gradually.

Fig 3.7: Sintering of electrodes in the furnace at 400 ° C

While the thickness and quality of TiO_2 film was verified with SEM, a quasi-transparent activated platinum layer was formed, on the surface of the counter electrode after sintering, as shown in the Figure 3.8

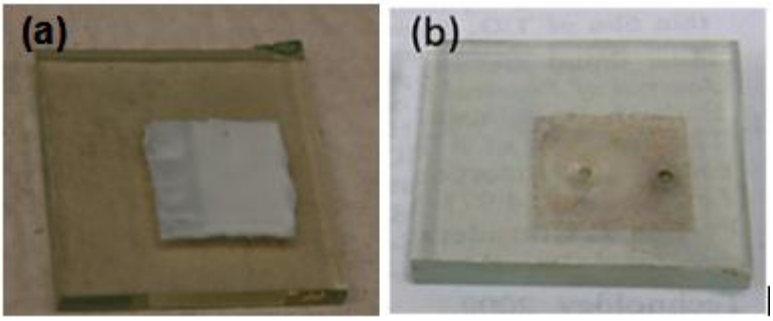

Fig 3.8: (a) Working electrode with sintered TiO_2 layer, (b) Counter electrode with quasi transparent activated platinum layer

3.2.5 N719 Dye Immersion

The annealed TiO_2 film was soaked in an ethanol solution of Ru (II)L2(NCS) 2 : 2 TBA (L=2,2′-bipyridyl-4,4′-dicarboxylate, TBA=tetra butyl ammonium, N719 Solaronix) overnight to absorb enough dye molecules into the porous TiO_2 matrix. To prepare the dye solution, 12.3 mg Ruthenium 535-bis TBA was added to 40ml pure ethanol to achieve the target concentration and was sonicated for 5 minutes (Figure 3.9 (a)) to properly disperse the dye molecules. TiO_2 electrode was immersed into the dye solution and kept for a period of 24 hours at room temperature. The container with dye solution was sealed with two layers of airtight wrap to avoid evaporation of the pure ethanol. After 24 hours, the TiO_2 film changed its color from white to a brown-red color as shown in Figure 3.9 (b), indicating successful absorption of the dye by the TiO_2 layer. The white dots on the TiO_2 layer are the aggregation of TiO_2 particles, which is a normal observation under higher magnification such as, the Keyence Scope.

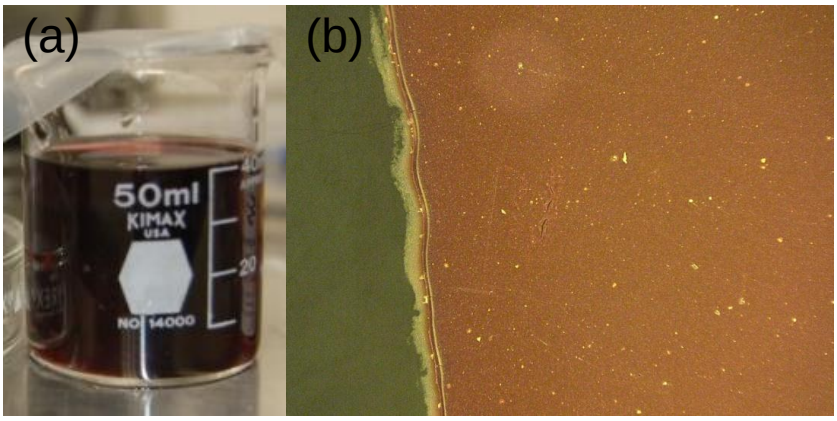

Fig 3.9 - (a) Image of N719 dye solution (b) TiO_2 layer after dye absorption under the Keyence Microscope.

3.2.6 Sealing Procedure of SX1170-PF25 sealant/Cell assembly

Proper sealing procedure can prevent the electrolyte from leaking or evaporating from the sandwiched layer of the cell. Efficient sealing also helps controlling the gap thickness between the electrodes. SX1170-25 (Surlyn, thickness 25µm, Solaronix) was used as the gasket between electrodes in this project. SX1170-25 with a 0.5 cm x 0.5 cm area was placed between two electrodes with two binder clips. However, poor sealing was observed using the smaller binder clips but the larger clips, which exerted more pressure, improved the sealing process. Finally using the larger binder clips was standardized for the fabrication process. The sealing process was performed at a temperature of 135^0 C for 12-14 minutes to melt the sealant completely. The calibration data of the furnace showed a 10^0 C difference between the LCD monitor of the furnace and the real temperature inside the furnace. Therefore, a temperature of 125^0 C was set to achieve 135^0 C temperatures inside the furnace. To check the leakage current after sealing, the resistance was measured using the ohm meter by putting two probe tips on the conductive layer of both electrodes. With a constant voltage input and over 2M ohm resistance reading represented an ultra-low leakage which confirmed no direct contact between the conductive layers of both electrodes.

Fig 3.10: Assembling the cell with binder clips for Sealing

3.2.7 Electrolyte Injection

The electrolyte (Iodolyte Z-150, Solaronix) was injected through the hole from counter electrode by using a syringe. There is a possibility of air bubbles getting trapped in the cell which was avoided by applying higher injection force. Electrolyte droplets were injected using a general syringe into the cell prepared as shown in the Figure 3.11. Injection process was repeated to avoid dry-out and bubbles. The electrolyte filling process stands completed once the bubbles inside the cell disappear. One hole with a bigger diameter than the size of the needle was used but a long injecting time was needed. Higher force could effectively push the air out of the DSSC to complete the electrolyte injection but might damage the TiO_2 layer. A hole on the TiO_2 layer corresponding to the location of the injecting hole on the counter electrode was observed on a DSSC when electrolyte injection took place several times. Extra care was taken to avoid the needle touching the TiO_2 layer during the injection.

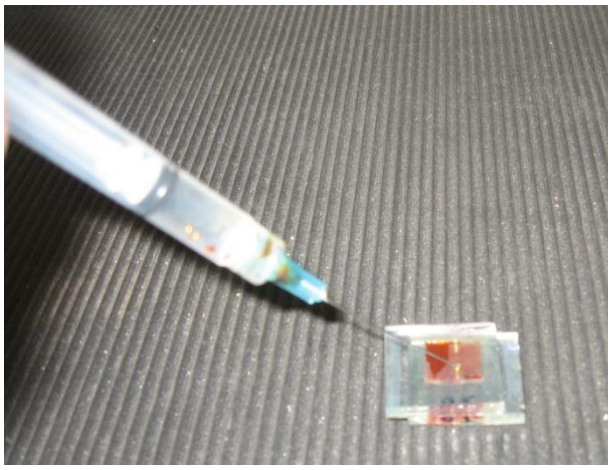

Fig 3.11: Electrolyte injection with Syringe

3.2.8 Hole Sealing

To avoid evaporation of the electrolyte, the hole on the counter electrode was immediately sealed after injection of the electrolyte. The hole sealing process was accomplished by using a hot gel gun as shown in the Figure 3.12 (a). The hot gel gun required six minutes to pre-heat before it could be used. The gel was then placed on top of the hole to complete the sealing process as well as the fabrication of the DSSC.

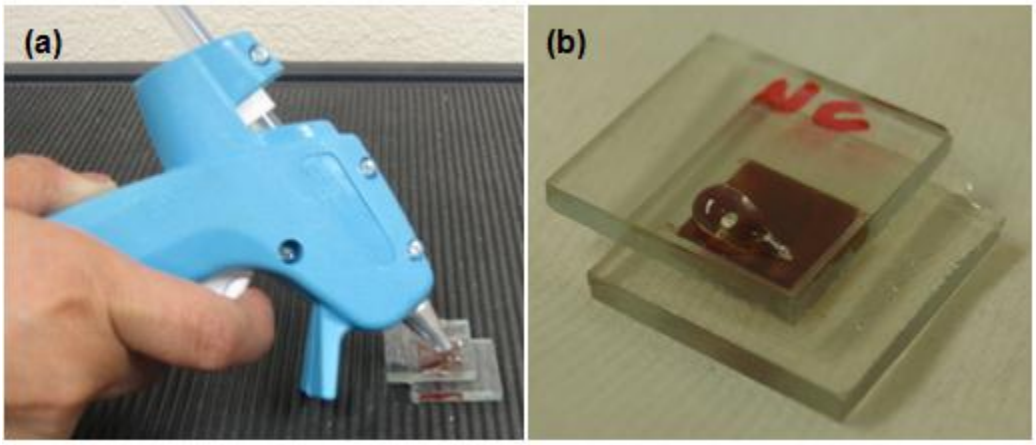

Fig 3.12: (a) Sealing the hole with hot gel gun (b) Fabricated DSSC

3.2.9 Evaluation of DSSC

Oriel 500W Universal Lamp Housing with F/1 (UV grade fused silica collimating condenser) and 150 W Xe OF Arc Lamp (Newport), was used to simulate the sun light with AM 1.5 and powered by Newport Arc Lamp Power Supply Model 69907 (Figure 3.13 (a)) Parstat 2273 Advanced Electrochemical System (Figure 3.13 (b)) was used to measure the I-V curve and the impedance plot (Nyquist plot). The DSS cell parameters, Voc, Isc, and FF were extracted from the I-V curve to determine the DSSC efficiency and the Nyquist plot revealed the internal resistances of the DSSC. To receive 100mW/cm^2 irradiance from the solar simulator light source, the DSSC was placed on the stage and adjusted its height under the light source. The height of the stage for the measurement was adjusted by using the reference cell based on NREL standards. The crocodile clips were used to connect the anode and cathode side of the DSSCs for measurement.

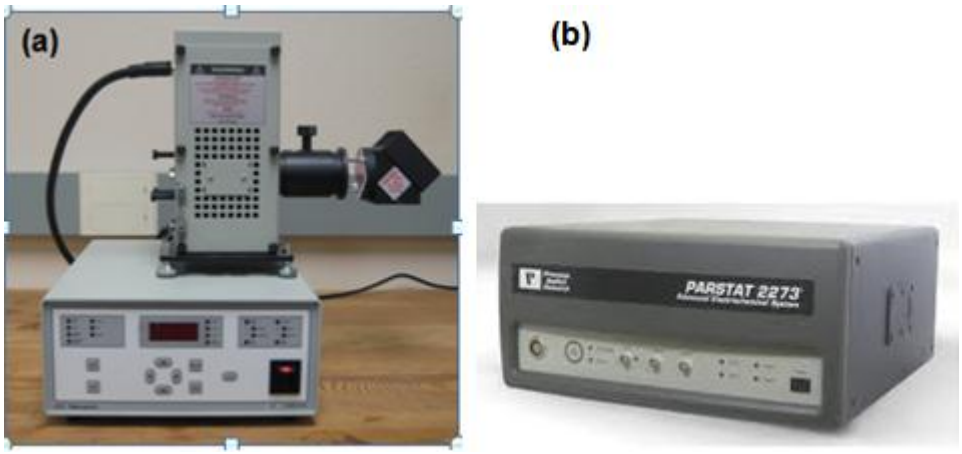

Fig 3.13: (a) Solar Simulator (b) Advanced Electrochemical System

To measure the I-V curve, the input voltage was swept from V_{oc} to 0 V with a 10 mV interval to collect the corresponding current. The increasing current was observed with a decreasing voltage to measure the I-V curve. While measuring the Nyquist plot, the DC voltage was set up at Voc point with a 10mV AC voltage. The scanning frequency range was from 100Hz to 1MHz to collect the internal impedance from three semi-circles generated during testing of the DSSC.

3.2.10 DSSC Measurement procedure for I-V curves and Z plots

1. The DSSC cell efficiency is determined using the cell parameters V_{oc}, I_{sc} and FF(Fill factor) as shown in the equation given below:

$$\eta = I_{sc} * V_{oc} * FF$$

These DSS cell parameters are extracted from the I-V curve. To receive 100mW/cm^2 irradiance from the solar simulator light source, the DSSC cell is placed on the stage and the height of the stage is adjusted under the light source.

2. Calibration of the stage: In order to avoid any errors in the measurements of I-V Curves, calibration of the solar simulator was carried out. The power of solar simulator was adjusted with the photocurrents of the reference cells. Action spectra of the amorphous Silicon solar cell and DSSC are similar to each other. Amorphous Silicon solar cell (reference cell) was taken from photovoltaic testing laboratory at ASU for carrying out calibration. This was carried out to minimize the spectral mismatch between solar simulator and natural sun illumination.
3. Power suite software: This software is used as the interface between PARSTAT and solar simulator to measure the efficiency and plot the I-V curves.

3.3 Description of Research Methods & Experiments

The three phases of the experiments conducted are described below:

3.3.1 Modifications to Standard Fabrication process

The fabrication process passed through several different versions. With each version, we have observed and recorded an increased stability and higher efficiency in the cells.

3.3.1.1 Changes made to Electrode cutting process

The glass electrodes required for DSSCs were being cut using the diamond wheel saw. This cutting process was effective in cutting process resulting in clean finish cut electrodes but was not efficient and it was also very time consuming. To enhance the efficiency, laser cutting machine from Universal was used as shown in the figure 3.14 Corel draw software helped to make the required line diagram for the cutting process.

The laser used the print function on the software to cut the electrodes of dimension (1.25 cm x 1.25 cm) as defined in Corel draw.

Fig 3.14: Cutting of glass electrodes using Laser (Universal Laser system)

3.3.1.2 Changes made to sealant cutting process

Proper sealing procedure can prevent the electrolyte from leaking or evaporating from the sandwiched layer of the cell. Efficient sealing also helps in controlling gap thickness between the electrodes. SX1170-25 (Surlyn, thickness 25µm, Solaronix) was used as the gasket between electrodes in this project. SX1170-25 with a 0.5 cm x 0.5 cm area was placed between two electrodes with two binder clips to complete the sealing process of the two electrodes. The sealant size variation range was from 0.5 to 0.7 cm. The sealant size variation was taken into account to find the right dimension so that the sealant can cover maximum surface area of the electrodes. It is essential that more surface area of the coated part of the electrode is covered with electrolyte to enhance the cell efficiency. On the other side, it is imperative that the sealant cross-section doesn't get expanded beyond the requirement after the sealing process resulting in the leaking of electrolyte, and the cell becoming non-functional.

The previous version of fabrication process used the laser machine to cut the 25 micron thick sealant to the required dimensions as defined by the Corel draw software.

Typically the dimension of the sealant cross –section should be smaller than the coated electrode area. It was observed that laser doesn't have enough movement to provide a resolution required for the cross section. The power of the laser also varied with usage, which resulted in improper cross sections for the sealant. On investigation, it was also found that use of laser was over melting the cross section edges resulting in higher dimension on one side. This process induced high stress at the cross-section edges and damaged the sealant quality. The deformed sealant material contributed to the weaker sealing between the sandwiched electrodes. This also led to formation of air pockets around the area creating hindrance to injection of electrolyte to cover the whole coated area after the sealing process. It was observed that many cells with such configuration were non-functional and showed less or no efficiency. At times some such cells seemed to work with expected results.

This particular procedure introduced lot of variability in the process. So there was a need to change the way the sealant was cut to improve the output of the process as well as the repeatability of the process.

The new way of cutting the sealant was developed. To avoid the limitations created from the above process, the sealant cutting process was changed to a more manual but an effective process. The sealant was cut into dimensions of (2.2 cm X 2.2 cm). In order to cut the sealant cross section of dimensions (0.6 cm x 0.6 cm), the said dimension engraving was made on the plastic substrate by creating grooves along the dimensions of the sealant. This substrate formed the default for all the sealant process. The cut sealants were placed on the square cut on the substrate. The sealant was made firm on the substrate by the scotch tape along the sides of the sealant. The X-Acto knife(X3601) was used to cut the sealant by moving along the grooves made on the substrate to arrive at the specified sealant dimensions. After this process, the scotch tape supporting the sealant was carefully removed from the substrate without exerting high pressure on the sealant. This is a very critical step.

Fig 3.15: Modified Sealant cutting process

3.3.2 Sputtering platinum on the counter electrode

The literature suggests that platinum sputtering offers more uniform coating of the platinum on the counter electrode than doctor blade coating. However, the sputtering experiments conducted in our lab did not provide adequate roughness and transparency required for efficient operation of the DSSC and consequently the cell performance diminished compared to manual coating of the platinum layer.

In dye-sensitized solar cells (DSSCs), counter electrode is an important component and its role is to transfer the electrons from external circuit back to the electrolyte and catalyzing the reduction of triiodide. Therefore, a counter electrode with high electrochemical activity is indispensable to fabricate an efficient DSSC.

Platinum is widely used material as a counter electrode due to its superior electro catalytic activity. Many materials have been dealt with like carbon, graphene and other conducting polymers, which reduce the cost of the counter electrodes. According to the literature, these materials have shown less performance compared to the platinum. Different methods of coating are in use like electro deposition, chemical reduction and sputtering. In sputter deposition method, the elements, which will give a better result, will be maintaining a lower deposition rate will yield greater uniformity, placing samples far from the source will help uniformity, but will also lower the deposition rate, controlling deposition rate, which depends on the position and orientation of the glass substrate in the chamber.

Figure 3.16 below shows the SEM picture of the platinum sputtered counter electrode. This image is taken from one of the cited research work [119].

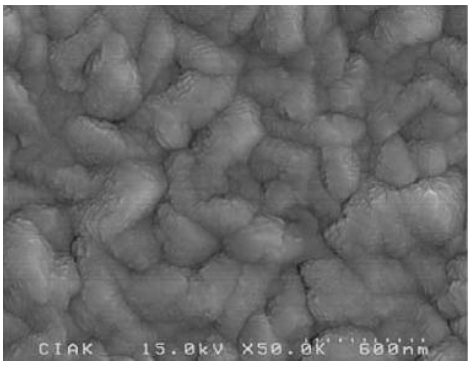

Fig 3.16: FESEM of Platinum sputtered counter electrode [119]

Figure 3.16 shows the FE-SEM image of the sputtered Pt electrode surface. Pt was deposited as a thick film on rough FTO surface, and its thickness was approximately 0.5 μm. It was observed that the sheet resistance of the Pt sputtered film was measured as 4–5 ohm/sq and is smaller than that in the case of doctor blade method.

The experimental study was carried out to analyze and study the effects of sputtering on platinum counter electrode. In this study we investigated the initial stability of DSSC with two Pt counter electrodes prepared by sputtering and default doctor blade coating method used in our fabrication process. The results are described here.

Experimental setup:

For the sputtering process, EDWARDS S150B sputtering machine was used. Pt films were deposited on ITO substrates (8 Ω/□, Solaronix Co., Ltd) using a DC sputtering equipment. The deposition was performed with a sputtering current in the range of mA under a base pressure of 10^{-2} mbar. The voltage was kept at 0.75kV for all the sputtering experiments. Flow of argon gas inside the chamber was controlled to generate sustained plasma.

Fig 3.17: Edwards S150B sputtering machine

Thin Pt films of various thicknesses were prepared by controlling the deposition time in the sputtering process. The Pt coated ITO substrates were used as counter electrodes to assemble the DSSCs and the performances of these cells were measured under one sun illumination (AM 1.5, 100 mW/cm^2).

Parametric configurations:

For achieving different thicknesses of platinum layer, the power was kept same but the sputtering time was varied from 30 - 120s, (with 30 seconds intervals) and 120-240s (Using 60 second intervals). Different combinations were experimented to confirm the uniformity of the layer.

Sputtering procedure: The steps to carry out the sputtering of sample inside the EDWARDS S150B equipment are as under:

1. Close the pressure control and gas/air admittance valves by turning the knobs clockwise.
2. Put the specimen to be coated into the holder and place the holder on the work table.
3. Press the main button (R.P).The pump starts and pirani gauge is switched on.
4. Wait for the chamber to be evacuated to a pressure less than 10^{-1}mbar.
5. Gradually open the pressure control needle valve until the pressure rises to $3x10^{-1}$ mbar.

6. Set H.T voltage to the scale reading determined in advance.
7. Set the time for sputtering.
8. Press the H.T button. The H.T indicates lamp lights and the glow discharge strikes the chamber. Check the current meter, which indicated the required current (40 mA). Press the timer button. Rate of deposition was approximately 15 nm /minute.
9. When the time has elapsed, the time button switched off the HT and the glow discharge is terminated.

3.3.3 Applicability of SWCNT in working electrode

The use of SWCNT as a conducting support for the working electrode is well documented. They discuss different methods of mixing SWCNT with TiO_2 material uniformly. The SWCNT used in the project was commercially obtained from the Cheap tubes (2-30 μm and 1-2 nm outer diameter) .The procedure followed in this project was to mix the carbon nanotubes directly with the TiO_2 paste.

The aggregation of SWCNTs was broken into tiny particles by ultrasonicating the composition of ethanol and carbon nanotubes in a small glass vial for a period of 5 minutes. To make the TiO_2-SWCNT composite, different amounts of pure ethanol with SWCNTs, as shown in the table, were poured into the TiO_2 paste and the mixture was stirred with the help of magnetic stirring for a period of approximately 2 hours. The prepared TiO_2 paste was then coated on the working electrode using the Coatema tool.

SWCNT loading	**0.1 wt. %**	**0.2 wt. %**	**0.4 wt. %**
TiO_2 Paste	**1000 mg**	**500 mg**	**250mg**
Ethanol amount	**0.1 ml**	**0.1ml**	**0.1 ml**
SWCNT amount	**0.1 mg**	**0.1mg**	**0.1mg**

Table 2: Different Weight percent loading

The color difference of the TiO_2 film with different SWCNTs loadings was observed visually. After sintering the working electrode, the TiO_2 layer with a higher SWCNT loading (Figure 3.18, 0.4 wt. % SWCNTs) showed a light blue color, compared

to the white color in the STD cell. After assembling these cells, I-V curves and Nyquist Plots were measured to investigate the effect of SWCNTs on cell efficiency.

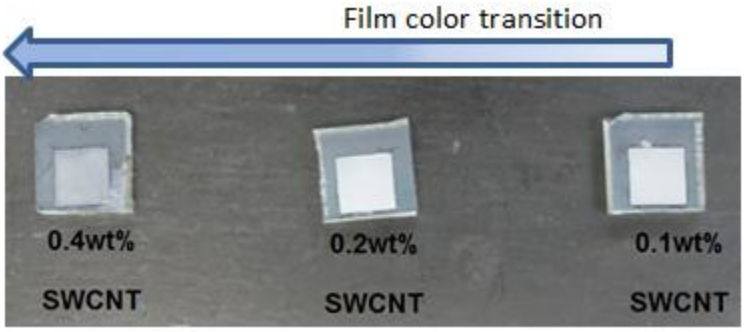

Fig 3.18: Color change with SWCNT loading

4. RESULTS & DISCUSSION

4.1 Observation of results – Electrode cutting process

The shift in the process for cutting glass electrodes from the previous method of diamond saw wheel to laser cutting method had substantial and recognizable improvement in terms of cycle time of the fabrication process of dye sensitized solar cell.

The diamond saw wheel cutting process though highly effective but was very time consuming. The electrode cutting process using the laser tool reduced the time for cutting the electrodes (16 electrodes) from approximately 2 hours to about 30 minutes. Additionally, it helped in making precision cuts of the smaller electrodes in less time compared to the diamond cutting process, approximately 90 minutes to (16 electrodes) about 20-30 minutes. Overall, the implementation of laser cutting process of the electrodes showed a time improvement of 75% to prepare the electrodes.

4.2 Observation of Results – Modification to Standard Fabrication process

Even though the uniformity in coating was achieved, the efficiencies obtained after the assembly had considerable variations. The previous versions of the fabrication procedure had gone through several revisions and changes to make the process more automated with fewer problems. The final process step of the DSSC is mostly a manual process and requires perfect dextral coordination to accomplish best results and is heavily human dependent. This was achieved by carrying out repeated trials of the manual stages. Another main concern with the process was the yield and repeatability of the process. The work carried out looked into different ways to achieve higher throughput and repeatability in process.

Reproducibility is another criterion, ie. ability of an experiment or study to be accurately reproduced, or replicated. Since this is also a part of the fabrication process, there was a need to find a way to achieve this factor of performance in the process.

However, while carrying out the DSSC process, it was found that the process was not that reproducible in terms of having variations in the cell efficiency and also the

yield of the cells fabricated was minimal. In order to achieve the required efficiency and throughput for the process, all different process variables were tested. After conducting different set of experiments, it was observed that the sealant assembly process was generating the maximum variation and hence the sealing process was concentrated for improvement to achieve higher efficiency and yield of the DSSCs.

A new way of cutting the sealant for the DSSC assembly process was initiated. The results obtained after making this change were quite encouraging. The cells fabricated with the modified configuration showed better efficiencies in the range of 9.5% to 11.8%, which is an acceptable efficiency range for the DSSC compared to the standard fabrication procedure. Also it was observed that revised sealant cutting process improved throughput of the whole process in terms of number of working cells. The cell fabrication yield reached to 80%, which was much higher than the previous yield using the standard sealant cutting process

The figure 4.1 below shows the results obtained after implementing modifications described above in the process. The cell efficiencies calculated for the I-V curves shown in the figure 4.1 are in the range of 10-12%, and the current density ranges from 25 mA/cm^2 to 34 mA/cm^2, which is quite efficient in terms of reproducibility for cells. While the open circuit voltage varied from 0.68 V to 0.74 V.

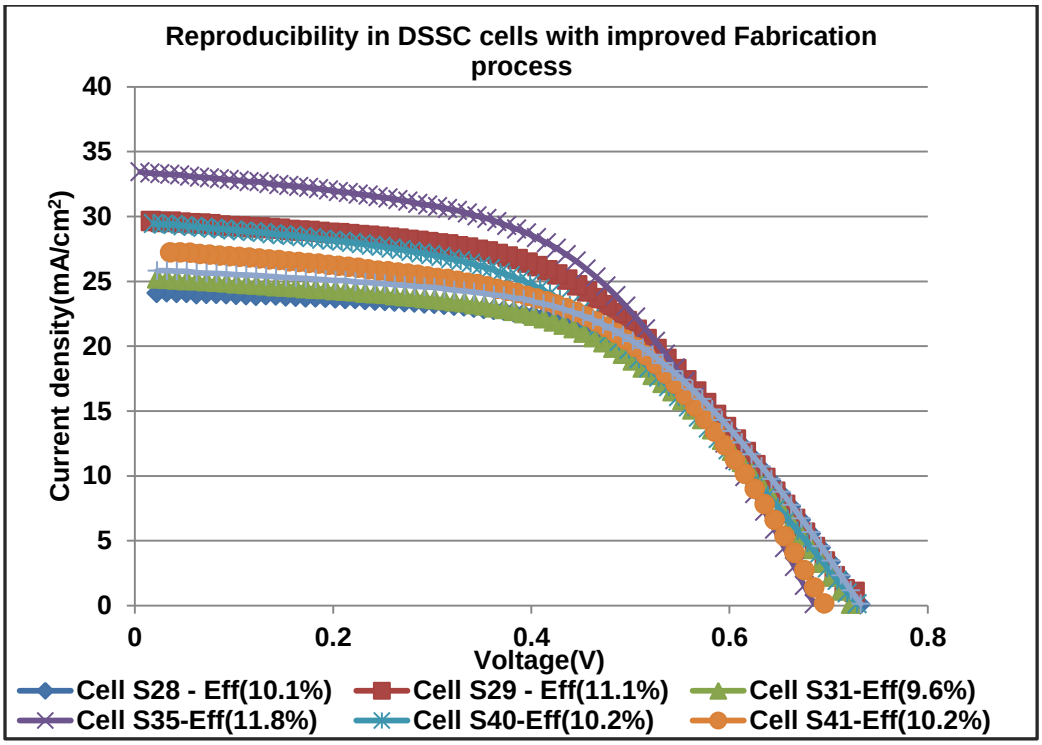

Fig 4.1 Cell efficiency to study the process repeatability

In order to confirm the repeatability in the process, a trend chart was plotted for these cells to find the time at which the efficiency got stabilized and whether those efficiency values are within the expected ranges. The fabricated cells were evaluated for efficiency with an interval of 3 days and the trend chart was plotted for these cells. It was observed that the efficiency of cells reached a saturation value within a period of 10 days. As can be seen from the trend chart that most of efficiency values are in the expected range. This improved fabrication process produced a maximum cell efficiency value of 11.8% in our laboratory to date. At the same time, the cell performance was also in range or slightly above the highest efficient cells reported in the literature.

One more investigation showed that the efficiency of cell reduced with time, and this was due to electrolyte evaporation, taking place in due course of time with exposure to UV light and wear and tear of cells.

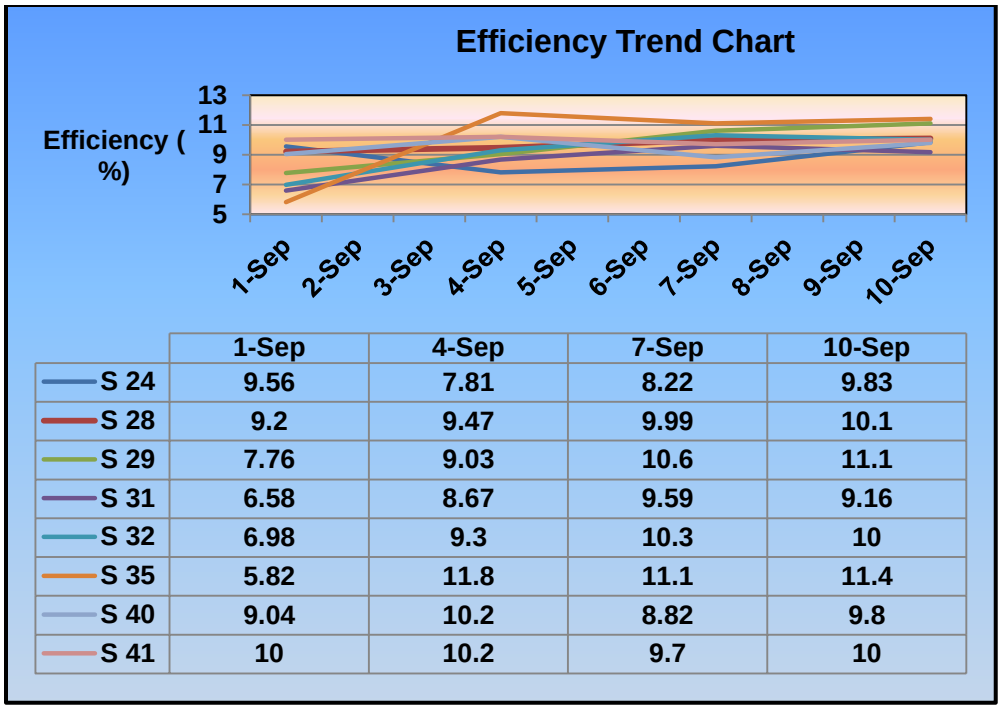

	1-Sep	4-Sep	7-Sep	10-Sep
S 24	9.56	7.81	8.22	9.83
S 28	9.2	9.47	9.99	10.1
S 29	7.76	9.03	10.6	11.1
S 31	6.58	8.67	9.59	9.16
S 32	6.98	9.3	10.3	10
S 35	5.82	11.8	11.1	11.4
S 40	9.04	10.2	8.82	9.8
S 41	10	10.2	9.7	10

Fig 4.2 Cell stability trend chart

4.3 Effect of sputtering platinum on the counter electrode

After carrying out different sputter time periods, DSSC cell was assembled using the fabrication method mentioned in the thesis. The Pt coated ITO substrates were used as counter electrodes to assemble DSSCs and the performance of these cells were measured under one sun illumination (AM 1.5, 100 mW/cm^2).

Classification of experiment: The experiments were carried out to analyze whether there is any effect on efficiency and stability of the cell by making use of platinum sputtered counter electrodes in fabrication.

The parameter used for sputtering experiments was sputtering time. Keeping the voltage and current at constant value, the time for sputtering was varied from 30 – 240 seconds. The rate of deposition of platinum on the glass substrate was dependent only on the sputtering time, voltage and current kept constant during the run. Since the two parameters of voltage and current were kept constant, time would determine the amount of deposition. The thickness of platinum layer was not measured due to unavailability of appropriate equipment for the same. But based on literature for the platinum sputtering

for the given set of conditions, the rate of deposition was estimated to be around 0.11 ± 0.005 nm /second. The uniformity of the layer was much better compared to coated version of platinum.

Table 3 shows the related parameters obtained from the I–V curves for two samples with different sputtering times. For the front-side illumination, no regular tendency was obtained for the variation of Isc, Voc, and fill factor with increase of Pt film thickness.

Cell Name	Time (secs)	Voc (V)	Isc (mA/cm2)	Efficiency (%)	Fill factor
Cell 1	120	0.72	9	2.34	0.36
Cell 2	240	0.8	15	6	0.5

Table 3: Parameters of Experiment

The table above shows the values measured after the fabrication process. With measurement of efficiency over a period of time, we observed a decreasing trend in performance of the cells.

Consider the first case of Cell 2:

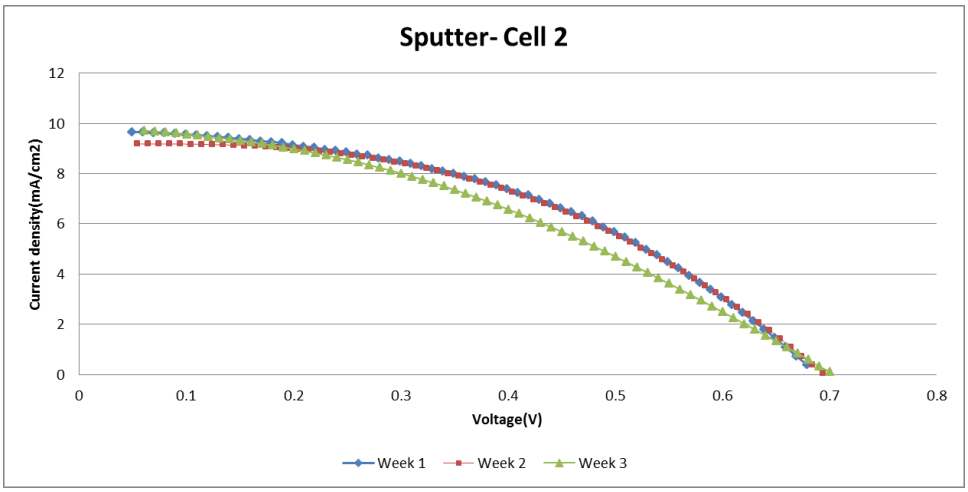

Fig 4.3: I-V curves trend of DSSC with sputtered platinum layer on the counter electrode.

The cell was monitored for period of three weeks and observed performance degradation in cells with increasing time. The fill factor of the cell is 0.36 which is a very

low value; fill factor determines the quality of the cell. The current density also decreased with time even though we find the open circuit voltage remained at a constant value with time. Following graph shows the efficiency trend of the above cell.

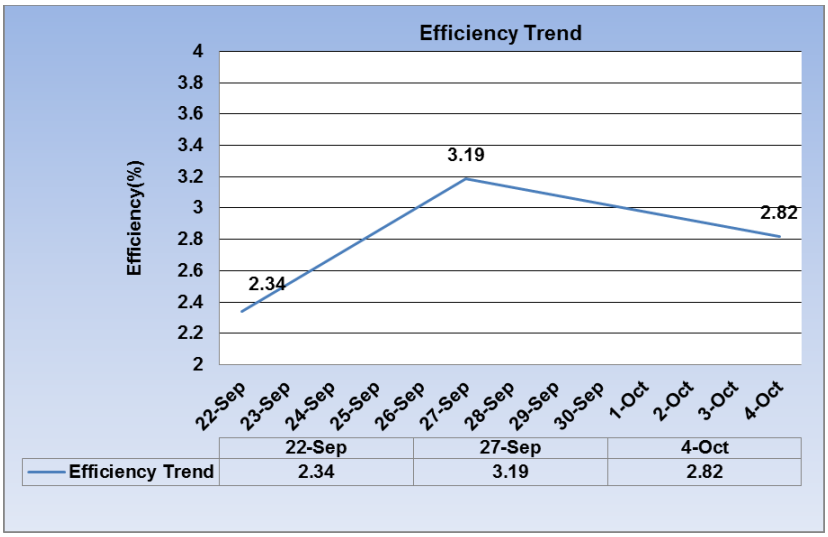

Fig 4.4: Cell 2 Efficiency trend

With degrading performance, further monitoring of the cell was stopped. In order to investigate the root cause that is causing these problems, sputtering time was increased to 240 seconds thinking that the amount of platinum deposited on the counter electrode might not be adequate for the cell operation.

Case of Cell 1: The main motivation is to achieve stability and reach good efficiency of cells and the platinum sputter deposition as an alternative was implemented to study the effects and ascertain whether sputtering process is beneficial to the DSSC fabrication as well as performance.

Below figure shows the I-V curves for cell 1 and its periodical changes in performance.

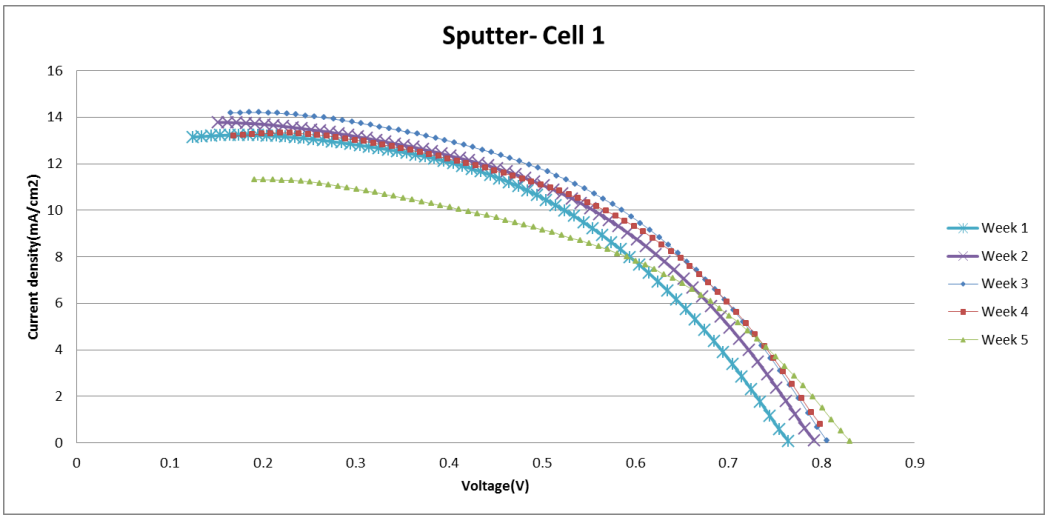

Fig 4.5: I-V Curve of the sputtered platinum cells

Again here we observe that the fill factor is low but compared to above cell it is much better. With periodical measurement, current density decreased, affecting the efficiency of the cell. This may be due to the increase in the internal resistance of the cell. The efficiency trend is as shown below:

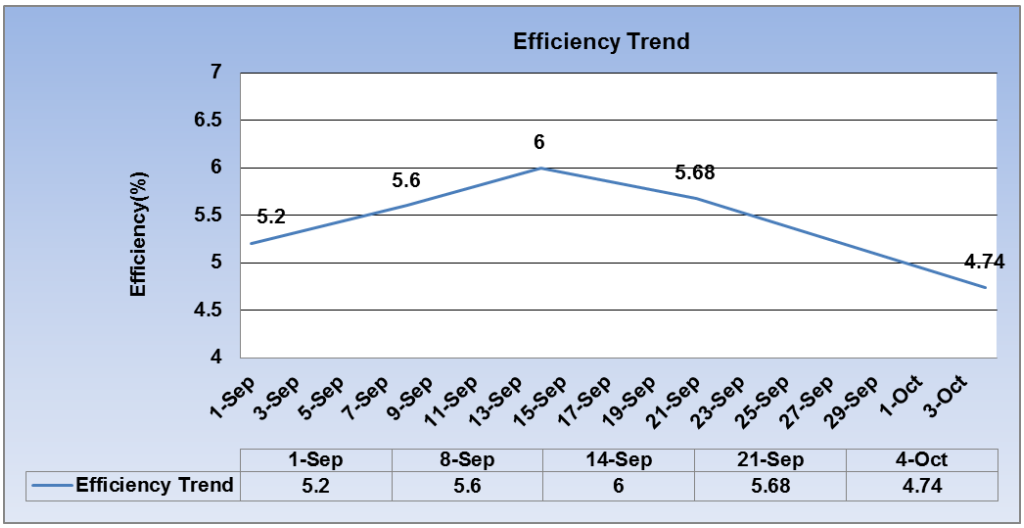

Fig 4.6: Cell 1 Efficiency trend

The efficiency was monitored for a period of 1 month, which is a sufficient period to assess the stability of the cell. In order to understand the effects of platinum counter electrode, the resistance or the Nyquist plot was plotted to compare the differences in

resistance between a coated and sputtered counter electrode, which gave lot of information.

Test condition	Remark
Frequency	100 - 10 MHz
Temperature	25 °C
DC Voltage	Voc
AC Voltage	10 mV
Rh	Sheet resistance of TCO
R1	Carrier transport resistance of Pt Electrode
R2	Carrier transport resistance of TiO2/dye/electrolyte interface
R3	Diffusion within electrolyte(Sealant THK)

Table 4: Cell impedance characteristics

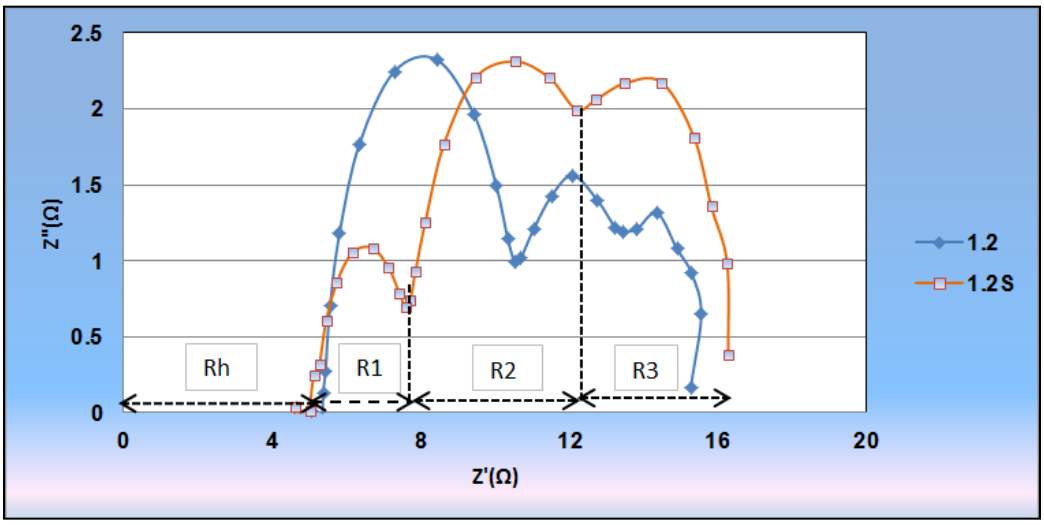

Fig 4.7: Impedance plot of platinum electrode (Doctor Blade (1.2) and Sputter (1.2S))

φ = 13 nm	Cell 1.2	Cell 1.2S
Rh	**5.38**	**4.65**
R1	**5.32**	**3.06**
R2	**3.13**	**4.48**
R3	**1.44**	**3.66**
Total (Rs)	**12.14**	**11.37**
Efficiency (%)	**7.49**	**5.68**
Voc (V)	**0.81**	**0.8**
Isc (mA.cm-2)	**19**	**11**
FF	**0.49**	**0.65**

Table 5: Impedance values for the Doctor Blade and Sputter cell

4.3.1 Discussion

The I-V measurement of DSSC was conducted after 24 h from the time of electrolyte injection to allow proper adhesion of the sealant. In the case of two Pt counter electrodes, the sputtered platinum electrode exhibited rapid degradation of efficiency with poor stability for only 3 days. Pt was deposited as a thick film on rough FTO surface, and its thickness was approximately calculated based on deposition rate. The sheet resistance of Pt sputtered film was measured as 4–5 ohm/sq. This is smaller than that in the case of a coated Pt substrate.

In the EIS (Electrochemical Impedance Spectroscopy) experiment, there is no significant change in impedance characteristics in doctor blade coated platinum electrode for more than a week. However, in the case of sputtered Pt electrode, three times increase in the value of series resistance was recorded. This increase in resistance is due to degradation of adhesion between Pt and TCO layers. Therefore, the high stability of the interface between counter electrode and substrate is found to be one of important factors for enhancing the stability of DSSC.

It was also concluded that bombarding of platinum ions on the conducting glass substrate might have damaged the conducting coating on the glass and consequently affected negatively the conductivity and resistance of the glass substrate. Bombarding the substrate with high energy ions increases the temperature of the substrate eroding the tin oxide coating on the glass, losing the connection path.

4.4 Effect of SWCNT-TiO_2 composite with different loadings on Dye sensitized solar cell

The cells were fabricated with the procedure discussed in the previous chapter. Investigation of the cells fabricated using this mixture has produced interesting results to be discussed. The main motivation of this study was to understand the effects of SWCNT on DSSCs in terms of efficiency. Major information, which was observed during this part of study, was the effect of SWCNT on open circuit voltage (Voc) and fill factor of the cell.

Figure 4.8 shows the comparison of efficiencies for different SWCNT loading with the new standard cell fabrication process. New standard cell represents the cells

fabricated using the modified process of sealing in the DSSC assembly process. The cells with different loadings of SWCNT have also been fabricated with the modified fabrication procedure.

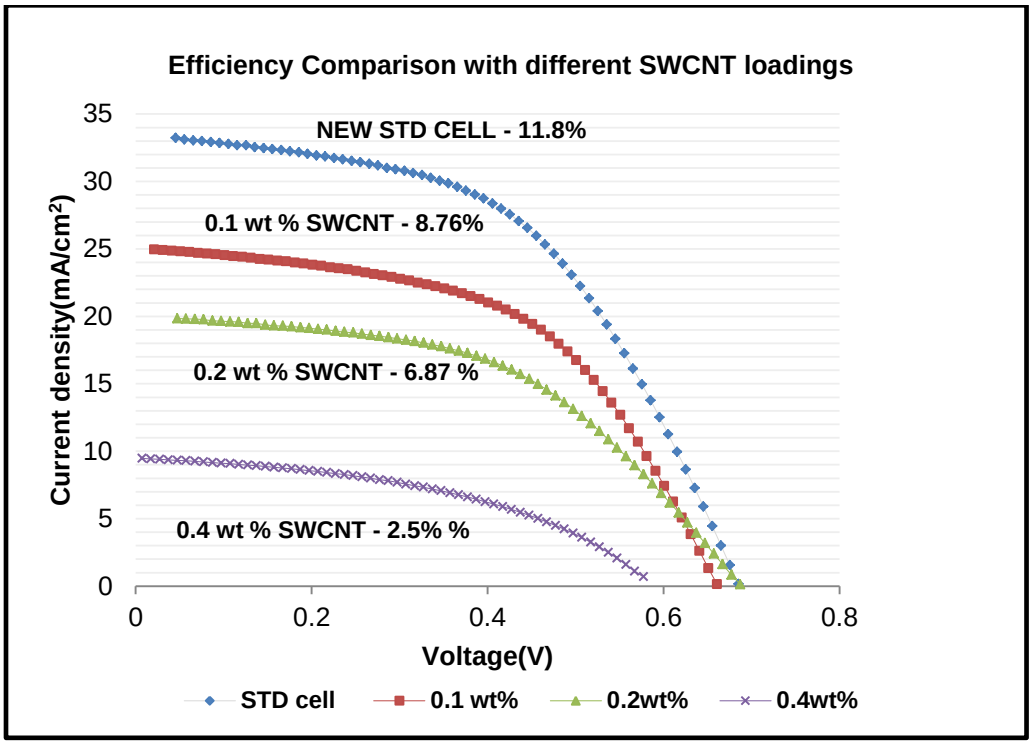

Fig 4.8: Efficiency comparison with different SWCNT loadings

As seen in the figure 4.8, the cell efficiency with 0.1 wt. % SWCNT loading is about 8.76%, which is quite comparable with the efficiency of the new standard cell. As the efficiency value of the DSSC gradually saturated to a value in the range of 10.4% to 11.4%. So we can conclude that the efficiency values of 0.1 wt. % are comparable to new standard cell efficiency. It was also found that the efficiency is decreasing about 25 % with increase in the weight percent of SWCNT.

Figure 4.9 shows the effect of SWCNT loading on open circuit voltage (Voc) and Isc. As it can be seen in the figure 4.9, with the increase in the SWCNT content in the TiO_2, the open circuit voltage of the cell decreases. It is seen that for 0.1 wt. % loading, the open circuit voltage is in the range of 0.68-0.70 volts. For 0.2 wt. % loading, with

period of observation, the open circuit voltage lies in the range of 0.64- 0.66 volts. For 0.4 wt. %, it was observed that there is a sudden drop in the open circuit voltage (Voc) .The value of open circuit voltage drops to a range of 0.48 -0.55 volts. The range of open circuit voltages was collected for different sets of cells with different SWCNT loadings. The figure below gives information on three cells with 0.1/0.2/0.4 wt. % loading observed for a period of time. The values provided here are for the cells observed over an interval period of every two days.

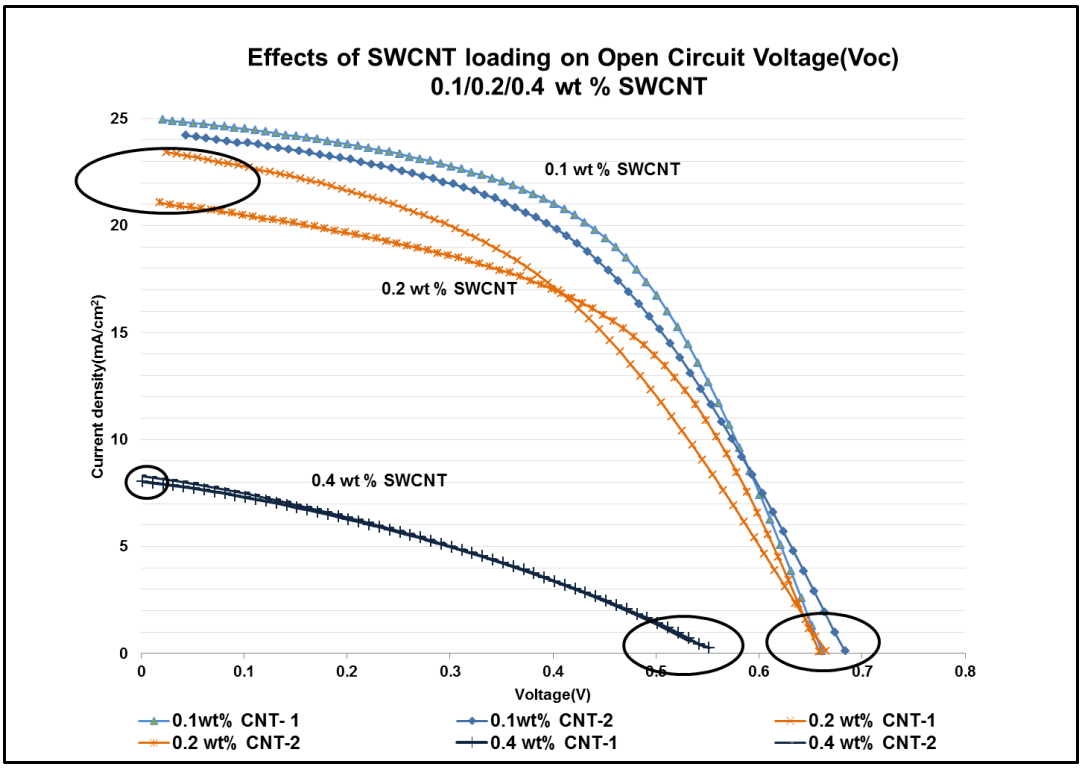

Fig 4.9: Effect of SWCNT loading on Open circuit voltage (Voc)

Next important result, which was found on investigation, was the effect of SWCNT on the fill factor of the cell. It was found that SWCNT has a degrading effect on the fill factor of the cell. Fill factor determines the quality of the cell. Figure 4.10 shows the comparison of fill factor for different weight loadings of SWCNT in TiO_2.It can be seen from the figure 4.10, that fill factor decreases with increased loading of SWCNT from 0.1 wt % to 0.4 wt. %.From the figure, it is observed that fill factor for the 0.1 wt. % SWCNT is 0.53. While for 0.2 wt. % loading, the fill factor is 0.47. This is 11 % decrease in the fill

factor of the cell. The 0.4 wt. % loading shows a dip in the fill factor by about 27 %, which is quite low compared to the new standard cell, hence providing significantly lower efficiency.

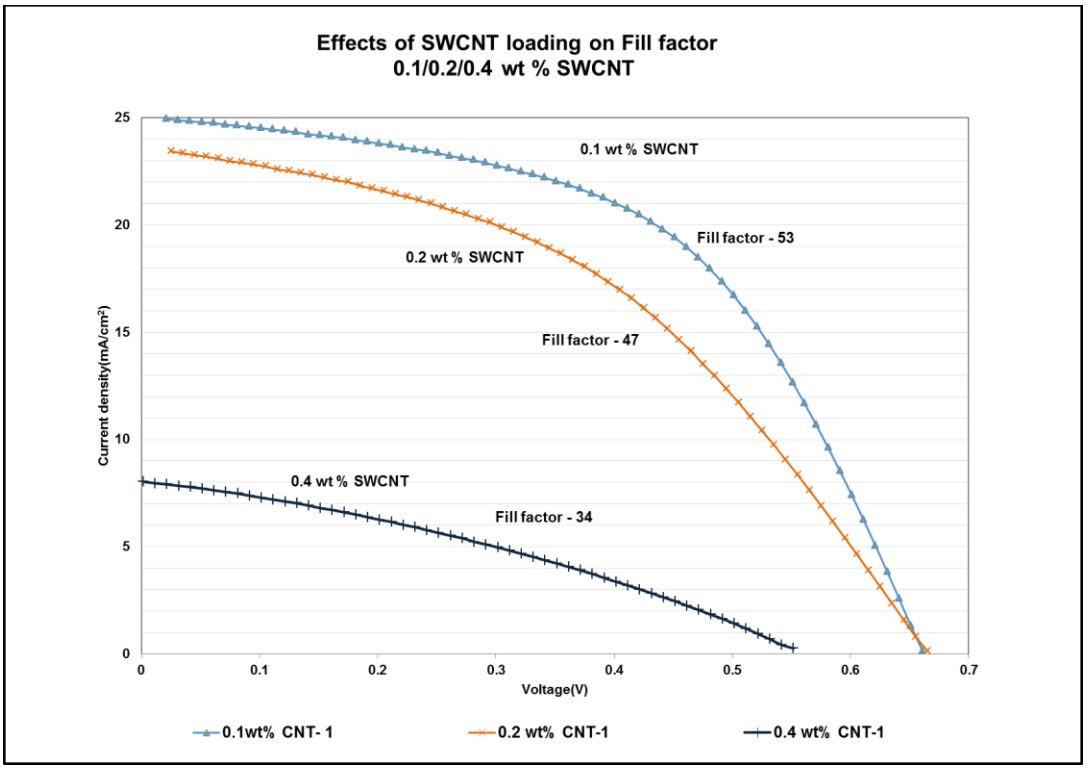

Fig 4.10: Effects of SWCNT loading on Fill factor of DSSC

4.4.1 Nyquist Plot of DSSCs with Different SWCNT loadings

The equivalent circuit of DSSCs was analyzed by using Electrochemical Impedance Spectroscopy (EIS) technique. The Nyquist plot measured by EIS technique revealed the internal resistances of the DSSC. Figure 4.11 (a) is an example of the Nyquist Plot, measured by the EIS method to interpret the internal resistance of DSSCs

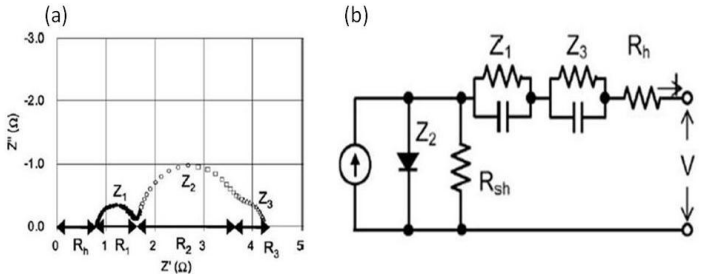

Figure 4.11: (a) Nyquist plot and (b) Equivalent Circuit of DSSC [122]

Three semicircles were observed in the measured frequency range from 100Hz to 1 MHz and R_h, which locates high frequency range > 10^6 Hz area, represents the sheet resistance of the TCO substrate and is primarily influenced by the thickness of the conductive layer on the electrode. R_1 is related to the carrier transport resistance at the surface of Pt counter electrode and can be varied changing the roughness factor of counter electrode. R_3, which represents the diffusion of iodide and triiodide within the electrolyte, can be optimized by changing the distance between TCO and Pt counter electrode. R_2 shows the resistance of the TiO_2/dye/electrolyte interface in DSSCs, and reflects the properties of the photo-injected electrons within the TiO_2.

Table 6 shows the summary of DSSC internal resistance obtained by Nyquist plot. These are the cells fabricated using the new modified fabrication process and also keeping the default parameters constant. The only variation is the SWCNT-TiO_2 composite. The table shows the comparison of standard cell with SWCNT loaded cells. The series internal resistance, Rs, is defined as the sum of the resistance R_1, R_3, and R_h.

φ = 20 nm	STD cell	0.1 wt.% CNT	0.2 wt.% CNT	0.4 wt.% CNT
Rh	8.96	19.82	30.72	28.27
R1	0.69	3.83	4.01	111.85
R2	1.15	9.78	9.39	15.81
R3	0.95	1.43	1.14	14.22
Total(Rs)	10.6	25.08	35.87	154.34
Efficiency (%)	11.4	8.97	6.87	2.5
Voc (V)	0.72	0.68	0.63	0.48
Isc (mA.cm-2)	24	24	20	9
FF	0.55	0.53	0.47	0.34

Table 6: Summary of Internal resistance in DSSC with different SWCNT loadings

Figure 4.12 shows the Nyquist plot for the standard cell, figure 4.13 shows the Nyquist plot for cells with SWCNT loading (0.1 wt.% and 0.2 wt.%) and figure 4.14 shows the Nyquist plot for loading (0.4 wt.% SWCNT).

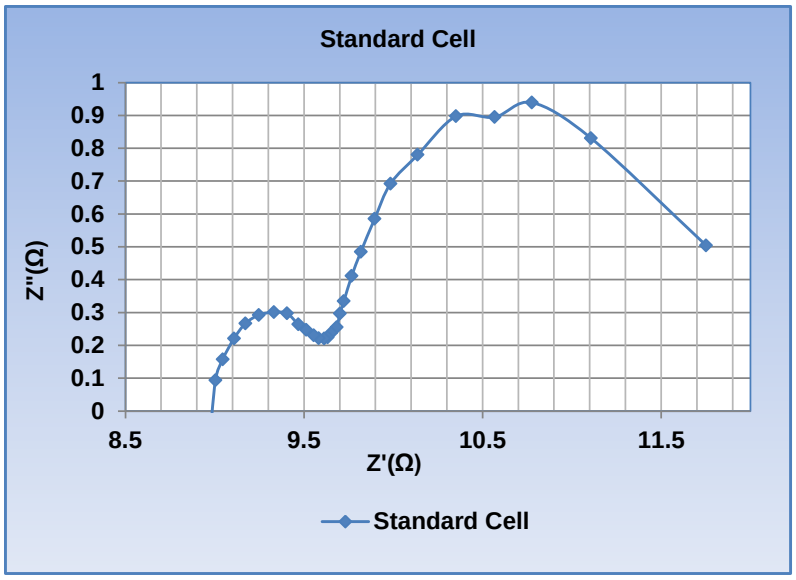

Fig 4.12: Nyquist plot for standard cell

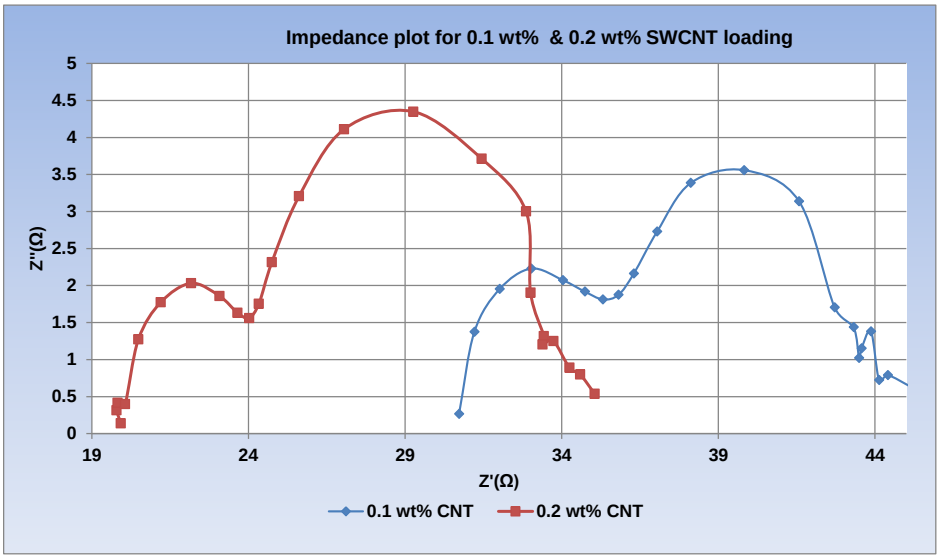

Fig 4.13: Nyquist plot for SWCNT loading (0.1 wt. % & 0.2 wt. %)

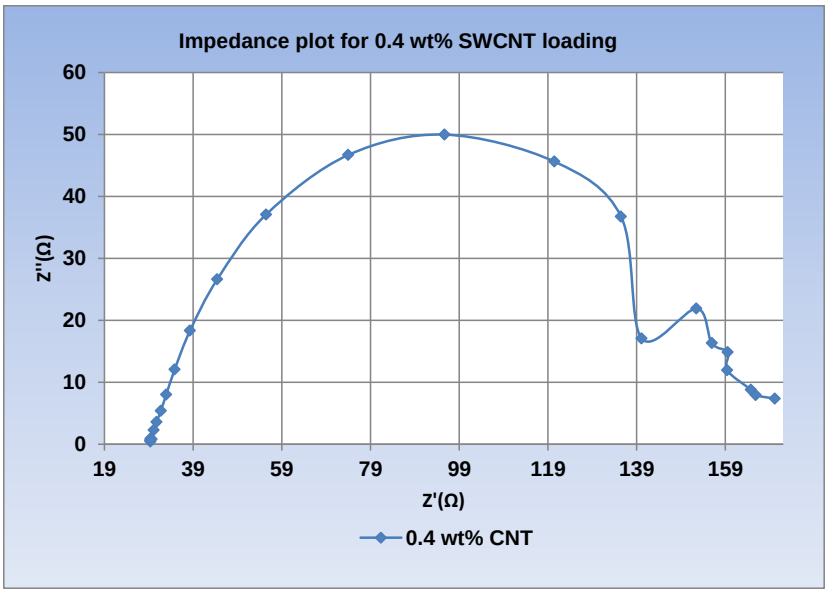

Fig 4.14: Nyquist plot for SWCNT loading (0.4 wt. %)

It is revealed in the table 6, as the loading of SWCNT increases, the series resistance of the cell increases. When compared with standard cell, the series resistance of the cells with SWCNT loading increased with increase in weight percent. This increase in series resistance decreases the efficiency of cells. Figure 4.15 shows the variation of open circuit voltage and series resistance with different SWCNT loading in comparison to the standard cell.

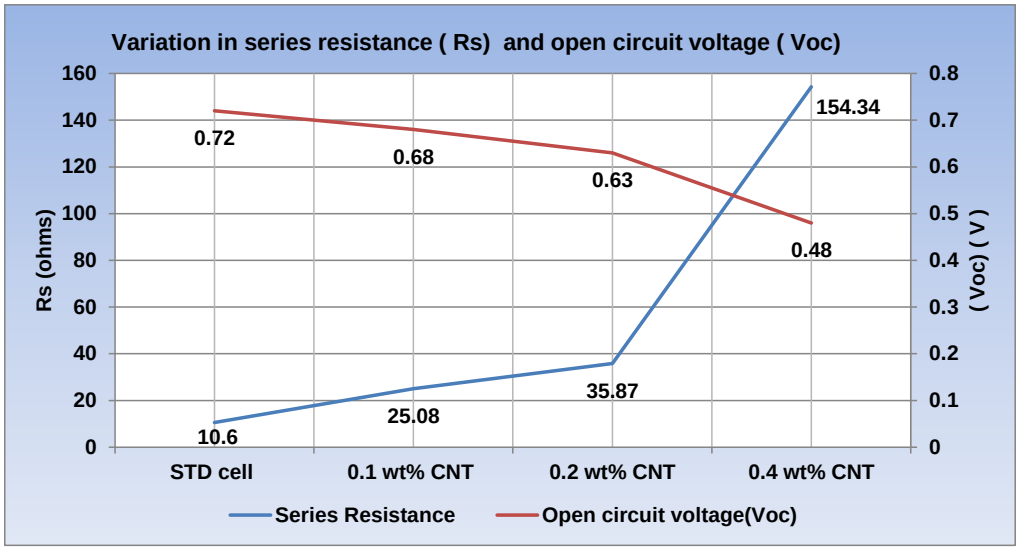

Fig 4.15: Variation in series resistance and Open circuit voltage

The above data was collected by carrying out experiments with different loadings of SWCNT within the TiO_2 coating. It was observed that both open circuit voltage and photocurrent were found to have measurable dependence on the TiO_2 layer loading. Photo voltage ranged from ~0.73 V to ~0.43 V and correspondingly photocurrent ranged from ~8 to ~33 mA depending on weight percent loading. It was observed that with increase in the loading, the series resistance increased substantially resulting in decrease of efficiency.

4.4.2 Discussion

The results obtained by carrying out these experiments gave enough insight to look into factors and mechanisms, which might be causing these degrading effects. A major difficulty in attaining higher photo–conversion efficiency in nanostructured glass electrodes is the transportation of electrons across the particle network formed due to SWCNT-TiO_2 composite. It is also known that the photo generated electrons in mesoscopic films have to travel through the network of semiconductor particles, during which these photo generated electrons encounter grain boundaries and as a result their transportation mobility suffers within the semiconducting layer of the cell. Having such random and unusual transit path for the photo generated electrons increases the probability of their recombination with oxidized sensitizer. The TiO_2 film particles undergo charge separation upon excitation with UV light (Eg> 3.2 eV).These photo anodes particulate films or TiO_2 films are coated on glass electrode surface exhibit anodic photo current generation. The magnitude of photocurrent describes the charge collection efficiency of the electrode surface.

It was also observed that with the increase in TiO_2 loadings, there is a decrease in the photo current. One reason for this behavior is that the particles aggregate and most TiO_2 aggregate particles are not able to connect with SWCNT. Since with higher TiO_2 loadings, it is seen that the color of the film became blue, which marks the transparency loss leading to saturation in the photo current, limiting the light absorption within the TiO_2 film.

As the photo injected electrons are transferred to TiO_2 from excited ruthenium complex, they undergo charge equilibration with SWCNT. This charge equilibrium is associated with the apparent Fermi level shift to more positive potentials. [120,121]. A positive shift to hundreds of millivolts in the apparent Fermi level was observed in the research publications from the redox equilibration experiments. This shift causes the open circuit voltage of the cell, which is influenced by difference in the Fermi levels between the photo anode and the redox couple, to be lower than that obtained in the absence of SWCNT. The SWCNT with TiO_2 helps in quick transport of electrons but at the expense of low open circuit voltage (Voc).

The Efficiency (η) defines the performance of DSSC, which is a function of open circuit voltage (V_{OC}), I_{SC} and the fill factor of the cell. Efficiency degradation was observed with increase in loading. This was mainly due to transparency loss of the TiO_2 working electrode and increase in series resistance of the cell. Increasing the fill factor can yield significant performance improvement of the DSSC.

$$FF = \frac{I_{max} \cdot V_{max}}{I_{sc} \cdot V_{oc}}$$

As Fill factor is the ratio of the maximum power to the external short and open circuit values, it is dependent on series resistance (R_s) and shunt resistance (R_{sh}). To obtain high fill factors, R_s has to be as small as possible, while R_{sh} needs to be as high as possible. The fill factor of the cell decreased with increase in SWCNT loading. Further investigations could be done in terms of lower loading of SWCNT to study any performance improvements in Dye sensitized solar cell.

5. CONCLUSION

5.1 General

DSSCs have attracted a lot of attention as potential low-cost alternative for single or polycrystalline p-n junction silicon solar cells. The main motivation for extensive research in this field is to make it commercial ready in order to compete with conventional silicon solar cell. The manufacturing cost of this cell is at least five times lesser than the conventional silicon solar cell. Several advantages including environmental cleanliness, working well under low-light condition and as an attractive alternative source of energy for portable application has grabbed the interests of research groups. Even though DSSCs are on the brink of commercialization, a few challenges still remain with major issues in sealing process leading to electrolyte evaporation, stability and long-term performance history. Controlling the internal resistance is one of the significant challenges to be solved.

The first objective of the project was to make the process reproducible and assess the throughput of the process. The changes made to fabrication process not only increased the efficiency of cells but it was seen that in one cycle of fabrication, yield of 90 % was achieved. The efficiency increased from the value of 11 % to 11. 8 %.

The second objective was to understand and analyze the effect of sputtering platinum on the counter electrode. After carrying out experiments and analysis, it was found that that bombarding of platinum ions on the conducting glass substrate is affecting the conductivity and resistance of the glass substrate. Bombarding the substrate with high energy ions is eroding the tin oxide coating on the glass, which deteriorates the layer leading to loss of conducting path in the circuit.

The third objective of the work studied was incorporation of SWCNT on the TiO_2 electrode and its effect on the cell efficiency. A major difficulty in attaining higher photo – conversion efficiency in nanostructured glass electrodes is the transportation of electrons across the particle network formed due to SWCNT-TiO_2 composite. It was also observed that with the increase in TiO_2 loadings, there is a decrease in the photo current. One

reason for this behavior is that the particles aggregate and most TiO_2 aggregate particles are not able to connect with SWCNT. Since with higher TiO_2 loadings, it is seen that the color of the film became blue, which marks the transparency loss leading to saturation in the photo current, limiting the light absorption within the TiO_2 film.

5.2 Specific recommendations

The experimental results demonstrated that higher internal resistance in the DSSCs was the origin for the reduced cell efficiency and direct mixing of SWCNTs had a negative effect on increasing the efficiency of DSSCs. In future works, several directions can be investigated. Firstly, making use of functionalized SWCNTs with TiO_2 mixture with different acid treatments can be experimented to compare and analyze the enhancement or the mechanism associated with the cell efficiency.

In the literature chapter, several acidic mixtures were experimented and obtained positive results in their DSSCs. However, it was not known what will happen if implemented with the same acidic mixture using SWCNT.

In addition, different ways to fabricate the CNT-TiO_2 layer are also intriguing directions to investigate for the reduction of internal resistances and the improvement of cell efficiencies. The approach we took in this project was the cost-effective approach.

Therefore, the enhanced efficiencies of DSSCs using different new materials like incorporating graphene into fabrication methods are worthy to pursue. Also, making the fabrication process automated to avoid the human error could be dealt with. Sealing process of the cell is critical to avoid electrolyte evaporation to maintain cell stability over a long period. The electrical contacts to the electrodes for cell characterization also need special attention. The current procedure has the liability of damaging the conductive coating on the electrode materials and better electrical contact with electrodes need to be explored. Also, new ways of platinum deposition could be implemented to compare performance characteristics and research into new materials to replace the platinum for counter electrode.

REFERENCES

[1] E. Becquerel. C R 1839, 9, 561.

[2] J. Simon and J.-J. André. Molecular Semiconductors: Photoelectrical Properties and Solar Cells Springer, 1985.

[3] D. Woehrle and D. Meissner. Adv Mater 1991, 3, 129.

[4] D. L. Morel, A. K. Kosh, T.Feng, et al. Appl Phys Lett 1978, 32, 495.

[5] C. W. Tang. Appl Phys Lett 1986, 48, 183-185.

[6] J. H. Schön, S. Berg, C. Kloc, et al. Science 2000, 287.

[7] J. H. Schön, C. Kloc, R. C. Haddon, et al. Science 2000, 288.

[8]. World Energy Council; 2004 Survey of Energy Resources, Oxford, 2004.

[9] S. Y. Lin, W. Y. Chou, “Investigation of Pentacene/Perylene Derivative Based Organic Solar Cells,” National Cheng Kung University, Tainan Tawian, 2007.

[10] Y. Chiba, A. Islam, Y. Watanabe, R. Komiya, N. Koide, and L. Han, “Dye-Sensitized Solar Cells with Conversion Efficiency of 11.1%,” *Japanese Journal of Applied Ph*ysic, vol. 45, pp. 638–640, 2006.

[11] Sterling, V.A. Planning and installing photovoltaic systems: a guide for installers, architects, and engineers; James & James / Earthscan, London, 2008.

[12] O’Regan, B.; Gratzel, M. Nature 1991, 353, 737-739.

[13] Nazeeruddin, M. K.; De Angelis, F.; Fantacci, S.; Selloni, A.; Viscardi, G.; Liska, P.; Ito, S.; Bessho, T.; Gratzel, M. Journal of American Chemical Society 2005, 127, 16835-16847.

[14] Hagfeldt, A.; Gratzel, M. Accounts of Chemical Research 2000, 33, 269-277.

[15] Yoon, C.H.; Vittal, R.; Lee, J.; Chae, W.S.; Kim, K.J. Electrochimica Acta 2008, 53, 2890-2896.

[16] Smestad, G.; Bignozzi, C.; Argazzi R. Solar Energy Materials and Solar Cells 1994, 32, 259-272.

[17] Bolton, J. R.; Hall, D. O. Photochemistry and Photobiology 1991, 53, 545.

[18] J. Moser. *Monatsh Chem* 1887, *8*, 373.

[19] H. Gerischer and H. Tributsch. *Berich Buns Gesell* 1968, *72*, 437-&.

[20] H. Gerischer, H. R. Schoppel and B. Pettinge. *J Electrochem Soc* 1972, *119*, C230.

[21] H. Tributsch and H. Gerischer. *Berich Buns Gesell* 1969, *73*, 251-&.

[22] R. Memming. *Faraday Discuss* 1974, 261-270.

[23] R. Memming and F. Schroppel. *Chem Phys Lett* 1979, *62*, 207-210.

[24] R. Memming, F. Schroppel and U. Bringmann. *J Electroanal Chem* 1979, *100*, 307-318.

[25] B. O'Regan and M. Grätzel. *Nature* 1991, *353*, 737-739.

[26]. Hauch, A.; Georg, A. Electrochimica Acta 2001; 46; 3457-3466.

[27] F. Cao, G. Oskam and P. Searson. *J Phys Chem* 1995, *99*, 17071.

[28] A. F. Nogueira, M. A. De Paoli, I. Montanari, et al. *J Phys Chem B* 2001, *105*, 7517-7524.

[29] W. A. Gazotti, A. F. Nogueira, E. M. Girotto, et al. *Synth Met* 2000, *108*, 151-157.

[30] W. Kubo, K. Muakoshi, T. Kitamura, et al. *Chem Lett* 1998, 1241.

[31] N. Papageorgiou, Y. Athanassov, M. Armand, et al. *J Electrochem Soc* 1996, *143*, 3099-3108.

[32] K. Tennakone, G. Kumara, I. Kottegoda, et al. *J Phys D-Appl Phys* 1998, *31*, 1492-1496.

[33] K. Tennakone, G. R. R. A. Kumara, A. R. Kumarasinghe, et al. *Semicond Sci Technol* 1995, *10*, 1689-1693.

[34] K. Tennakone, A. R. Kumarasinghe and P. M. Sirimanne. *Semicond Sci Technol* 1993,*Vol 8, Iss 8*, 1557-1560.

[35] K. Tennakone, G. R. R. A. Kumara, K. G. U. Wijayantha, et al. *Semicond Sci Technol* 1998, *13*, 134-138.

[36] B. O'Regan and D. T. S. D.T. *J Appl Phys* 1996, *80*, 4749.

[37] B. O‘Regan and D. Schwartz. *Chem Mater* 1998, *10*, 1501-1509.

[38] J. Hagen, W. Schaffrath, P. Otschik, et al. *Synth Met* 1997, *89*, 215-220.

[39] K. Murakoshi, G. Kano, Y. Wada, et al. *J Electronanal Chem* 1995, *396*, 27.

[40] K. Murakoshi, R. Kogure and S. Yanagida. *Chem Lett* 1997, *5*, 471-472.

[41] Sony corporation,"Research and development in DSSC , taking full advantage of materials".

[42] Planning and installing photovoltaic systems: a guide for installers, architects and engineers edited by Deutsche Gesellschaft für Sonnenenergie.

[43] Hasan Birk Gray , "The effects of platinum particle size to the efficiency
Of a dye sensitized solar cell (DSSC)" , pg 10-12.

[44] Jessica KRÜGER, Interface Engineering In Solid-State DSSC, University of Heidelberg, 2003.

[45] Michael Grätzel, "Photoelectrochemical cells," Nature, vol. 414, pp. 338-344, 2001.

[46] W. West, "First hundred years of spectral sensitization," Proc. Vogel Cent. Symp. Photogr. Sci. Eng., vol. 18, pp. 35–48, 1974.

[47] J. Moser, "Notiz über die Verstärkung photoelectrischer Ströme durch optische Sensibilisierung," Monatsh. Chem., 8, 373, 1887.

[48] Namba, S. & Hishiki, Y., "Color sensitization of zinc oxide with cyanide dyes," J.Phys. Chem., vol. 69, pp. 774–779, 1965.

[49] W. H. Brattain, C. G. B. Garrett, "Experiments on the interface between germanium and an electrolyte," Bell Syst. Tech. J., vol. 34, pp. 129–176, 1955.

[50] H. Gerischer, "Electrochemical behavior of semiconductors under illumination," J. Electrochem. Soc., vol.113, pp. 1174–1182, 1966.

[51] Michael Grätzel, "Review Dye-sensitized solar cells," Journal of Photochemistry and Photobiology C, Photochemistry Reviews, vol. 4, pp. 145–153, 2003.

[52] Hagfeldt, A.; Gratzel, M. Accounts of Chemical Research 2000, 33, 269-277.

[53] Hauch, A.; Georg, A. Electrochimica Acta 2001; 46; 3457-3466.

[54] Nazeeruddin, M.K.; Kay, A.; Rodicio, I.; Baker, R.H.; Muller, E.; Liska, P.; Vlachopoulos, N.; Gratzel, M. Journal of American Chemical Society 1993, 115, 6382-6390.

[55] Gratzel, M. Pure Applied Chemistry 2001, 73, 459–467.

[56] Smestad, G.P. Solar Energy Materials and Solar Cells 1998;55; 157-178.

[57] Tennakone, K.; Kumarasinghe, A.R., Kumara, G.R.R.A.,Wijayantha, K.G.U.; Sirimanne, P. M. Semiconductor Science,Technology 1995; 10 ; 1689-1693.

[58] Gratzel, M. Journal of Photochemistry and Photobiology A:Chemistry 2004; 164; 3-14.

[59] M. Toivola, L. Peltokorpi, J. Halme, P. Lund, “Regenerative effects by temperature variations in dye-sensitized solar cells,” *Solar Energy Materials & Solar Cells,* vol. 91, pp. 1733–1742, 2007.

[60] F. F. Santiago, J. Bisquert, E. Palomares, L. Otero, D. Kuang, S. M. Zakeeruddin, Michael Gratzel, “Correlation between Photovoltaic Performance and Impedance Spectroscopy of Dye-Sensitized Solar Cells Based on Ionic Liquids,” *J. Phys. Chem. C*, vol. 111, pp. 6550-6560, 2007.

[61] Functionalised carbon nanotubes as therapeutic vectors, Available at:http://www-ibmc.u-strasbg.fr/ict/vectorisation/nanotubes_eng.shtml

[62] R.Smalley, “Discovering the Fullerenes,” Rev.Mod.Phys, vol. 69, pp. 723–730, 1997.

[63] S.Iijima, “Helical Microtubes of Graphitic Carbon,” Nature, London, vol. 354, pp. 56-58, 1991.

[64] H.Rafii and Tabar, “Computational Physics of Carbon Nanotubes,” Cambridge, UK, vol. 1, pp. 12–18, 2008.

[65] A.Loiseau, P.Launois, and P.Petit, “Understanding Carbon Nanotubes,” Springer–Berlin, Heidelberg, pp. 1-50, 2006.

[66] M.S.Dresselhaus, G.Dresselhaus, J.C.Charlier and E.Hernandez, “Electronic, Thermal and Mechanical Properties of Carbon Nanotubes,” The Royal Society, London, pp. 1–34, 2004.

[67] Nazeeruddin, M.K.; Kay, A.; Rodicio, I.; Baker, R.H.; Muller, E.;Liska, P.; Vlachopoulos, N.; Gratzel, M. Journal of American Chemical Society 1993, 115, 6382-6390.

[68] Gratzel, M. Pure Applied Chemistry 2001, 73, 459–467.

[69] Keis, K.; Vayssieres, L.; Lindquist, S.E.; Hagfeldt, A. Nano Structured Materials 1999,12, 487-490.

[70] Hagfeldt, A.; Gratzel, M. Accounts of Chemical Research 2000, 33, 269-277.

[71] Lee, S.H.A.; Abrams, N.M.; Hoertz, P.G.; Barber, G.D.; Halaoui,L.I.; Mallouk, T.E. The Journal of Physical Chemistry B 2008,112 (46), 14415-14421.

[72] Gomez, M.; Magnusson, E.; Olsson, E., Hagfeldt, A., Lindquist,S.E., Granqvist, C.G. Solid State Physics 1999, 12, 146-149.

[73] O'Regan, B.; Gratzel, M. Nature 1991, 353, 737-739.

[74] Nazeeruddin, M. K. ; Pechy, P. ; Gratzel, M. Chemical Communications 1997, 18, 1705-1706.

[75] Ela, S.E.; Yilmaz, M.D.; Đcli, B.; Dede, Y.; Đcli, S.; Akkaya, E.U.Organic Letters 2009; 10 (15), 3299-3302.

[76] Kay, A.; Gratzel, M. Journal of Physical Chemistry 1993, 97, 6272.

[77] Kuang, D.; Walter, P.; Nuesch, F.; Kim, S.; Ko, J.; Comte, P.;Zakeeruddin, S.M.; Nazeeruddin, M.K.; Gratzel, M. Langmuir 2007, 23, 10906-10909.

[78] Smestad, G.P. Solar Energy Materials and Solar Cells 1998;55; 157-178.

[79] Hauch, A.; Georg, A. Electrochimica Acta 2001; 46; 3457-3466

[80] Kawano, R.; Matsui, H.; Matsuyama, C.; Sato, A.; Susan,M.A.B.H.; Tanabe, N., Watanabe, M. Journal of Photochemistry and Photobiology A: Chemistry 2004, 164, , 87–92.

[81] Peter L.M.; Duffy N.W.; Wang R.L.; Wijayantha, K.G.U. Journal of Electroanalytical Chemistry 2002, 524, 127-136.

[82] A.G. Osorio, I.C.L. Silveira, V.L. Bueno, C.P. Bergmann, "H_2SO_4/HNO_3/HCl-Functionalization and its effect on dispersion of carbon nanotubes in aqueous media," Applied Surface Science, vol. 255, pp. 2485–2489, 2008.

[83] X.H. Men, Z.Z. Zhang, H.J. Song, K. Wang, W. Jiang, Comp. Sci. Technol., vol.68, pp. 1042–1049, 2008.

[84] H. Kitano, K. Tachimoto, Y.J. Anraku, Colloid Interface Sci., vol. 306, pp. 28–33.

[85] J. Shen, W. Huang, L. Wu, Y. Hu, M. Ye, Comp. Sci. Technol., vol. 67, pp. 3041-3050, 2007.

[86] G.X. Chen, H. Shimizu, Polymer, vol. 49, pp. 943–951, 2008.

[87] X.L. Xie, Y.W. Mai, X.P. Zhou, Mater. Sci. Eng. R, vol. 49 pp. 89–112, 2005.

[88] J.J. Wang, G.P. Yin, J. Zhang, Z.B. Wang, Y.Z. Gao, Elect. Acta, vol. 52, pp. 7042-7050, 2007.

[89] Saito, R., Dresselhaus, G., and Dresselhaus, M. S. Physical Properties of Carbon Nanotubes, Imperial College Press, London, 1998.

[90] Javey, A. et al. Ballistic carbon nanotube field-effect transistors, Nature, 424,654, 2003.

[91] Iijima, S. Helical microtubules of graphitic carbon, Nature, 354, 56, 1991.

[92] Dresselhaus, M., Dresselhaus, G., and Avouris, P. Carbon Nanotubes: Synthesis, Structure, Properties and Applications, Springer-Verlag, Berlin, 2001.

[93] De Heer, W. A. Nanotubes and the pursuit of applications, MRS Bull., 29, 281, 2004.

[94] Zheng, M. et al. DNA-assisted dispersion and separation of carbon nanotubes,Nat. Mater., 2, 338, 2003.

[95] Krupke, R. et al. Separation of metallic from semiconducting single-walled carbon nanotubes, Science, 301, 344, 2003.

[96] Misewich, J. A. et al. Electrically induced optical emission from a carbon nanotube FET, Science, 300, 783, 2003.

[97] Li, J., et al. Bottom-up approach for carbon nanotube interconnects, Appl. Phys. Lett., 82, 2491, 2003.

[98] Yu, M.-F., Dyer, M. J., and Ruoff, R. S. Structure and mechanical flexibility of carbon nanotube ribbons: an atomic-force microscopy study, J. Appl. Phys.,89, 4554, 2001.

[99] Buongiorno Nardelli, M., Yakobson, B. I., and Bernholc, J. Mechanism of strain release in carbon nanotubes, Phys. Rev. B, 57, R4277, 1998.

[100] Solaronix Website, 2010, “Guide," Available:

http://www.solaronix.com/technology/guide/

[101] Sirbuly, D. J.; Law, M.; Yan, H.; Yang, P. J Phys. Chem. B 2005,109, 15190.

[102] Law, M.; Greene, L. E.; Johnson, J. C.; Saykally, R.; Yang, P.Nature Mater. 2005, 4, 455.

[103] Klimov, V. I. J. Phys. Chem. B 2006, 110, 16827.

[104] Mor, G. K.; Shankar, K.; Paulose, M.; Varghese, O. K.; Grimes,C. A. Nano Lett. 2006, 6, 215.

[105] Galoppini, E.; Rochford, J.; Chen, H.; Saraf, G.; Lu, Y.; Hagfeldt,A.; Boschloo, G. J. Phys. Chem. B 2006, 16159.

[106] Martinson, A. B. F.; Elam, J. W.; Hupp, J. T.; Pellin, M. J. Nano Lett. 2007, 7, 2183.

[107] Romanv, S. G.; Sotomayor Torres, C. M.; Yates, H. M.; Pemble,M. E.; Butko, V.; Tretijakov, V. J. Appl. Phys. 1997, 82, 380.

[108] Leschkies, K. S.; Divakar, R.; Basu, J.; Enache-Pommer, E.;Boercker, J. E.; Carter, C. B.; Kortshagen, U. R.; Norris, D. J.; Aydil, E. S.Nano Lett. 2007, 7, 1793.

[109] Girishkumar, G.; Hall, T. D.; Vinodgopal, K.; Kamat, P. V. J. Phys.Chem. B 2006, 110, 107.

[110] Kongkanand, A.; Vinodgopal, K.; Kuwabata, S.; Kamat, P. V. J.Phys. Chem. B 2006, 110, 16185.

[111] Kongkanand, A.; Domı´nguez, R. M.; Kamat, P. V. Nano Lett. 2007,7, 676.

[112] Vietmeyer, F.; Seger, B.; Kamat, P. V. AdV. Mater. 2007, 19, 2935.

[113] Hasobe, T.; Imahori, H.; Kamat, P. V.; Fukuzumi, S. J. Am. Chem.Soc. 2005, 127, 1216.

[114] Hasobe, T.; Kamat, P. V.; Troiani, V.; Solladie, N.; Ahn, T. K.;Kim, S. K.; Kim, D.; Kongkanand, A.; Kuwabata, S.; Fukuzumi, S. J. Phys.Chem. B 2005, 109, 19.

[115] Hasobe, T.; Fukuzumi, S.; Kamat, P. V. J. Am. Chem. Soc. 2005,127, 11884.

[116] Hasobe, T.; Fukuzumi, S.; Kamat, P. V. J. Phys. Chem. B 2006,110, 25477.

[117] Jung, K. H.; Hong, J. S.; Vittal, R.; Kim, K. J. Chem. Lett. 2002,864.

[118] Kongkanand, A.; Kuwabata, S.; Girishkumar, G.; Kamat, P.Langmuir 2006, 21,

2392.

[119] Bo-Kun Koo et.al “Seasoning effect of dye-sensitized solar cells with different counter electrodes” , J. Electroceram (2006).

[120] Kongkanand, A.; Kamat, P. V. ACS Nano 2007, 1, 13.

[121] Kongkanand, A.; Domı´nguez, R. M.; Kamat, P. V. Nano Lett. 2007,7, 676.

[122] L. Han, N. Koide,Y. Chiba, A. Islam, T. Mitate, “Modeling of an equivalent circuit for dye-sensitized solar cells: improvement of efficiency of dye-sensitized solar cells by reducing internal resistance,” ELSEVIER, C. R. Chimie, vol. 9, pp. 645–651, 2006.

APPENDIX

A. STEPS FOR CHARACTERIZATION USING POWER SUITE.

This section lists out the instructions and steps to carry out in the power suite software for the characterization of Dye sensitized solar cells.

Following are the sequence of steps, which are carried out in order to setup the power suite software for I-V measurements:

Step 1: The first step involves selecting the technique template, for I-V measurement choosing the cyclic polarization technique.

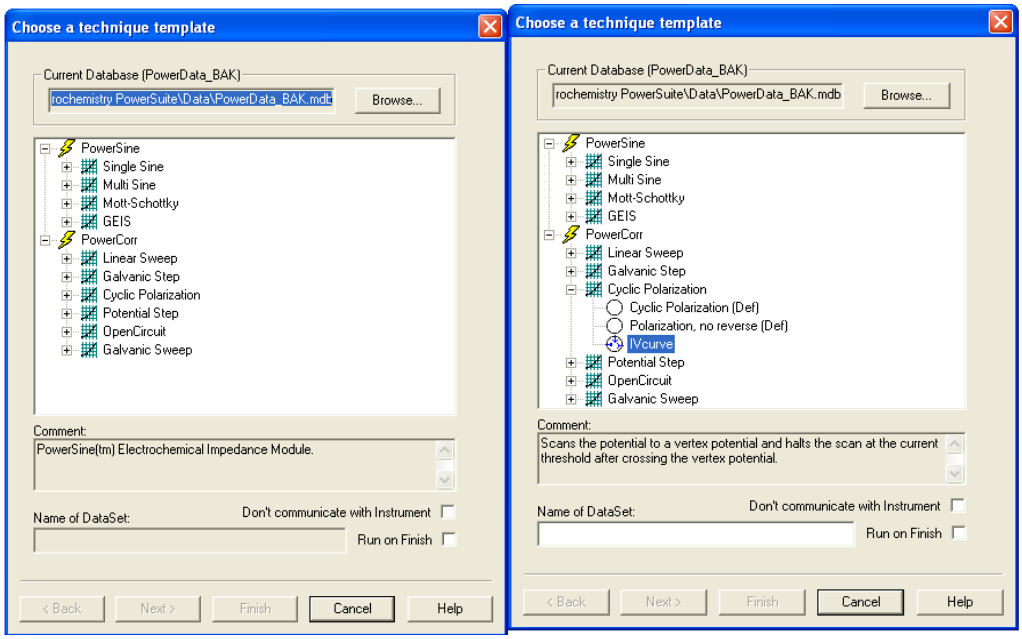

Fig A-1: Power suite technique template

Step 2: The measurement dataset is represented by an appropriate name to identify the measurements for a given cell.

Step 3: This step describes the cell definition which is characterized by the type of working electrode and the surface area of electrode which is filled with electrolyte solution is approximately 0.22 cm^2.

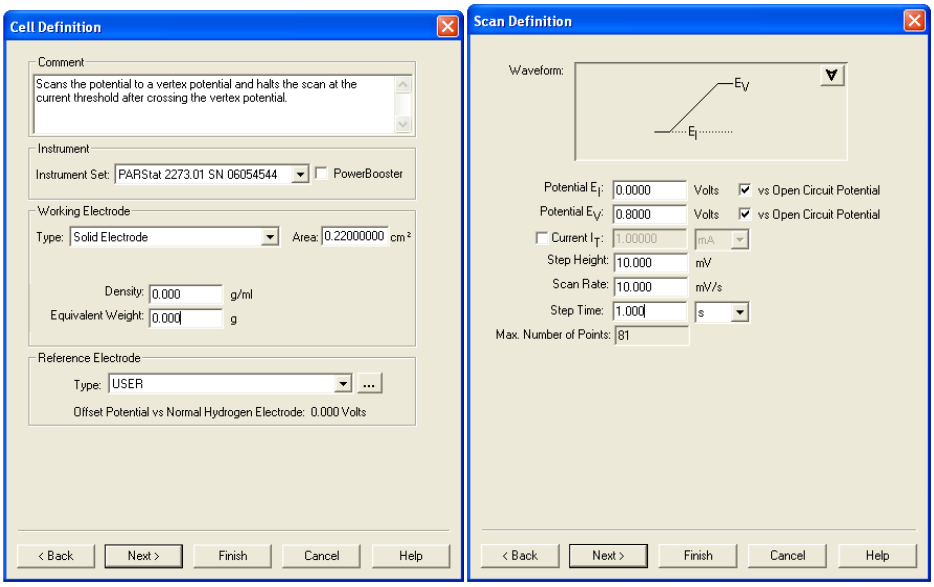

Fig A-2: Cell definition and Scan definition

Step 4: To measure the I-V curve, the input voltage was swept from V_{oc} to 0 V with a 10mV interval to collect the corresponding current. The Y axis is inverted to observe and record the proper required curve.

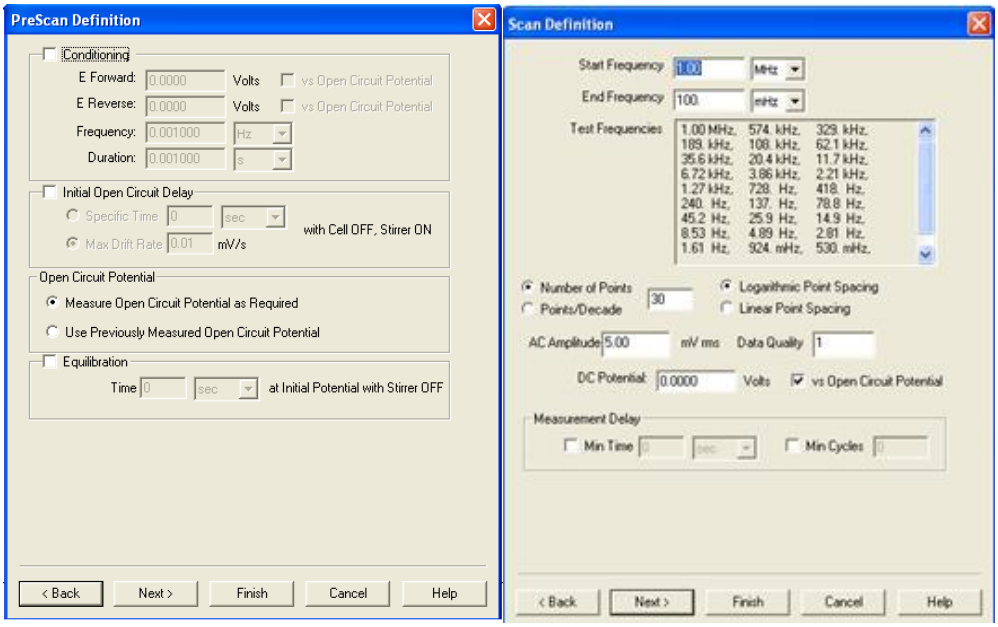

Fig A-3: Scan definition for EIS measurement

Step 5: Select external cell as the source cell for I-V measurements as the DSSC cell is connected with the crocodile clips.

Step 6: The setup is now ready for I-V measurements. Now press the go button with solar simulator in place with illumination and record the I-V curve plot.

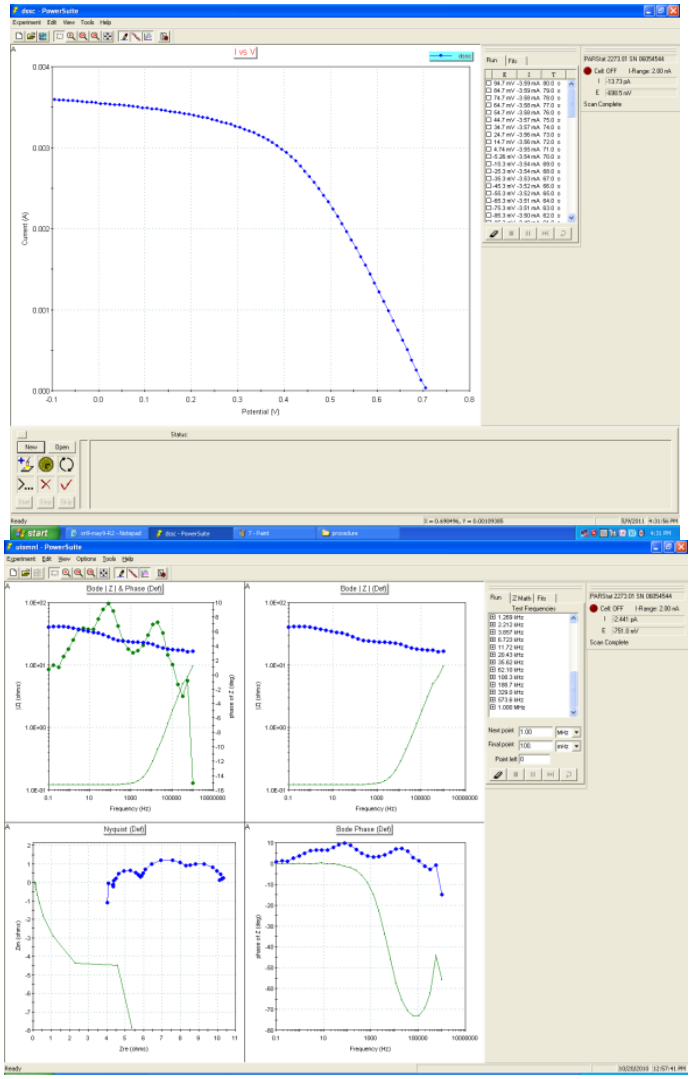

Fig A - 4: I-V Curve and Nyquist data

This summarizes the procedure for measuring the I-V curves of Dye sensitized solar cells.